12

DNA 4066F

STRESS-GAGE SYSTEM FOR THE MEGABAR (100 GPa) RANGE

Stanford Research Institute
333 Ravenswood Avenue
Menlo Park, California 94025

June 1976

Final Report for Period 13 August 1974—16 March 1976

CONTRACT No. DNA 001-75-C-0029

APPROVED FOR PUBLIC RELEASE;
DISTRIBUTION UNLIMITED.

THIS WORK SPONSORED BY THE DEFENSE NUCLEAR AGENCY
UNDER RDT&E RMSS CODE B344075462 J11AAXSX35220 H2590D.

Prepared for
Director
DEFENSE NUCLEAR AGENCY
Washington, D. C. 20305

Destroy this report when it is no longer needed. Do not return to sender.

UNCLASSIFIED

SECURITY CLASSIFICATION OF THIS PAGE (When Data Entered)

REPORT DOCUMENTATION PAGE

READ INSTRUCTIONS BEFORE COMPLETING FORM

1. REPORT NUMBER: DNA 4066F	2. GOVT ACCESSION NO.
3. RECIPIENT'S CATALOG NUMBER	
4. TITLE (and Subtitle): STRESS-GAGE SYSTEM FOR THE MEGABAR (100 GPa) RANGE	5. TYPE OF REPORT & PERIOD COVERED: Final Report for Period 13 Aug 74—16 Mar 76
	6. PERFORMING ORG. REPORT NUMBER: SRI Project PYU 3654
7. AUTHOR(s): P. S. De Carli, Author Contributors: D. C. Erlich, L. B. Hall, R. T. Bly, A. L. Whitson, D. D. Keough, D. R. Curran	8. CONTRACT OR GRANT NUMBER(s): DNA 001-75-C-0029
9. PERFORMING ORGANIZATION NAME AND ADDRESS: Stanford Research Institute 333 Ravenswood Avenue Menlo Park, California 94025	10. PROGRAM ELEMENT, PROJECT, TASK AREA & WORK UNIT NUMBERS: Subtask J11AAXSX352-20
11. CONTROLLING OFFICE NAME AND ADDRESS: Director Defense Nuclear Agency Washington, D.C. 20305	12. REPORT DATE: June 1976
	13. NUMBER OF PAGES: 80
14. MONITORING AGENCY NAME & ADDRESS (if different from Controlling Office): P. S. De Carli, D. C. Erlich, L. B. Hall, Rob Bly, Art Whitson	15. SECURITY CLASS (of this report): UNCLASSIFIED
	15a. DECLASSIFICATION/DOWNGRADING SCHEDULE

16. DISTRIBUTION STATEMENT (of this Report)

Approved for public release; distribution unlimited.

12 77p.

17. DISTRIBUTION STATEMENT (of the abstract entered in Block 20, if different from Report)

18. SUPPLEMENTARY NOTES

This work sponsored by the Defense Nuclear Agency under RDT&E RMSS Code B344075462 J11AAXSX35220 H2590D.

19. KEY WORDS (Continue on reverse side if necessary and identify by block number)

Manganin Gage
Megabar Stress Gage
Mutual-Inductance Particle Velocity Gage
Husky Pup Debris Coupling Experiment
Manganin Gage Calibration
EMP Hardening of Manganin Gage System

20. ABSTRACT (Continue on reverse side if necessary and identify by block number)

The useful range of the manganin piezoresistive stress transducer was extended from the former limit of about 45 GPa (450 kbar) to about 125 GPa (1250 kbar). The major problem encountered was shunting of the gage, caused by the increased electrical conductivity of insulators at high shock stresses. The effect of shunting was minimized through use of very-low-impedance (0.05 to 0.15-ohm) gages and through careful attention to gage geometry. Loading and release calibration data for manganin were obtained over the stress range 1187 Pages LB

DD FORM 1 JAN 73 1473 EDITION OF 1 NOV 65 IS OBSOLETE

UNCLASSIFIED

SECURITY CLASSIFICATION OF THIS PAGE (When Data Entered)

332500

20. ABSTRACT (Continued)

between about 25 and about 125 GPa. The results of earlier work, calibrations to 45 GPa, are critically reviewed. All of the reliable data on the dynamic piezoresistance of manganin can be fitted by the piecewise calibration curve,

$$P = \begin{cases} 42\ \text{GPa}\ (\Delta R/R_o) - 120\ \text{GPa}\ (\Delta R/R_o)^2, & P < 2\ \text{GPa} \\ 35\ \text{GPa}\ (\Delta R/R_o), & 2\ \text{GPa} \le P \le 15\ \text{GPa} \\ 48\ \text{GPa}\ (\Delta R/R_o) - 5.6\ \text{GPa}, & P \le 15\ \text{GPa} \end{cases}$$

A prototype high-stress mutual-inductance particle velocity gage was designed and tested. Six manganin gages, one background (unpowered manganin) gage, and one aluminum preheat temperature gage were fielded in the Debris Coupling Experiment of the Husky Pup nuclear event. Despite power supply failure, attributed to preshot flooding of the instrumentation alcove, excellent time-of-arrival data were obtained. These data disagree by about a factor of two with preshot predictions of shock-wave propagation in the Debris Coupling Experiment.

SUMMARY

The megabar (100 GPa) stress-gage work presented here was proposed in response to the Defense Nuclear Agency's need for the capability of making close-in free-field stress measurements in underground nuclear tests. In a previous DNA program under Contract No. DNA001-73-C-0225, we had determined that the piezoresistive response of manganin extended into the megabar range and that the problems of gage insulation and gage survivability were surmountable.

The present program consisted of five tasks:

(1) Design, construct, and test manganin gage packages that are adaptable to field use at very high stresses.

(2) Determine the effects of gage package and fabrication techniques on the response of the gage to stress above 40 GPa (400 kbar).

(3) Calibrate the manganin gage, for loading and release, over the stress range extending from about 40 GPa to 100 GPa.

(4) Design and construct a mutual-inductance particle velocity gage suitable for the high-stress region.

(5) Field six manganin gages in the debris coupling experiment of the Husky Pup nuclear event.

All of these tasks have been completed successfully. Manganin gage packages suitable for both laboratory and field use were tested over the stress range to 125 GPa. Loading and release calibration data for manganin were obtained over the stress range between about 25 and about 125 GPa. A prototype high-stress mutual-inductance particle velocity gage was designed and tested. Six active manganin gages, one background (unpowered manganin) gage, and one preheat temperature gage were fielded in Husky Pup.

In Husky Pup, the gage power supplies failed to operate (probably the result of preshot flooding of the alcove), but excellent time-of-arrival data were nevertheless obtained. A major conclusion from this experiment is that manganin gages are suitable for use in close-in measurements in the underground nuclear test environment.

Section II presents some general background material relevant to the use of laboratory Hugoniot data in computational predictions of material response to stress waves. Section III covers present work on the high-stress (to 125 GPa) calibration of manganin and also reviews previous work on manganin calibration below 40 GPa. Section IV is devoted to the mutual-inductance particle velocity gage. The Husky Pup Debris Coupling experiment is discussed in Section V. This section also includes results of laboratory measurements (granite conductivity at high shock stresses, response of in-granite gages, and response of manganin gage system to simulated EMP environment) that were made in support of Husky Pup. Appendix A is a brief description of all of the laboratory shock-wave experiments performed on this contract.

PREFACE

Lee Hall was responsible for all instrumentation work, including the design of the Husky Pup power supplies. James Dempster constructed the gage calibration assemblies and provided design assistance. Jim Yost, Darwin Henley, Frank Galimba, Ken Mock, Curt Benson, and Nick Pianca assisted with the experiments. Art Whitson and Rob Bly provided advice on EMP hardening of the gage system. Donald Curran, Carl Petersen (now at SSS) and Doug Keough were responsible for technical supervision of the project. Captain Jerry Stockton monitored the Husky Pup phase of the program; the gage development work was monitored by Col. Dan Burgess and Mr. Thomas Kennedy. Dr. Roy Shunk of SAI was a very constructive critic of the gage development work.

We are particularly indebted to Al Bartlett for his long hours of careful work in fabricating and assembling the Husky Pup granite cores.

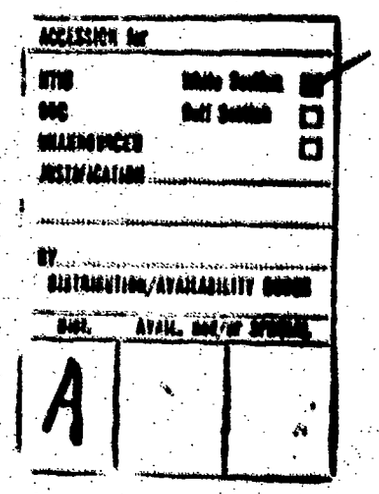

CONTENTS

LIST OF ILLUSTRATIONS

LIST OF TABLES

Table

CONVERSION FACTORS FOR U.S. CUSTOMARY TO METRIC (SI) UNITS OF MEASUREMENT

To Convert From	To	Multiply By
angstrom	meters (m)	1.000 000 × E -10
atmosphere (normal)	kilo pascal (kPa)	1.013 25 × E +2
bar	kilo pascal (kPa)	1.000 000 × E +2
barn	meter^2 (m^2)	1.000 000 × E -28
British thermal unit (thermochemical)	joule (J)	1.054 350 × E +3
calorie (thermochemical)	joule (J)	4.184 000
cal (thermochemical)/cm^2	mega joule/m^2 (MJ/m^2)	4.184 000 × E -2
curie	giga becquerel (GBq)*	3.700 000 × E +1
degree (angle)	radian (rad)	1.745 329 × E -2
degree Fahrenheit	degree kelvin (K)	$t_k = (t°f + 459.67)/1.8$
electron volt	joule (J)	1.602 19 × E -19
erg	joule (J)	1.000 000 × E -7
erg second	watt (W)	1.000 000 × E -7
foot	meter (m)	3.048 000 × E -1
foot-pound-force	joule (J)	1.355 818
gallon (U.S. liquid)	meter^3 (m^3)	3.785 412 × E -3
inch	meter (m)	2.540 000 × E -2
jerk	joule (J)	1.000 000 × E +9
joule/kilogram (J/kg) (radiation dose absorbed)	Gray (Gy)	1.000 000
kilotons	terajoules	4.183
kip (1000 lbf)	newton (N)	4.448 222 × E +3
kip inch^2 (ksi)	kilo pascal (kPa)	6.894 757 × E +3
ktap	newton-second/m^2 ($N-s/m^2$)	1.000 000 × E +2
micron	meter (m)	1.000 000 × E -6
mil	meter (m)	2.540 000 × E -5
mile (international)	meter (m)	1.609 344 × E +3
ounce	kilogram (kg)	2.834 952 × E -2
pound-force (lbf avoirdupois)	newton (N)	4.448 222
pound-force inch	newton-meter (N-m)	1.129 848 × E -1
pound-force/inch	newton/meter (N/m)	1.751 268 × E +2
pound-force foot^2	kilo pascal (kPa)	4.788 026 × E -2
pound-force/inch^2 (psi)	kilo pascal (kPa)	6.894 757
pound-mass (lbm avoirdupois)	kilogram (kg)	4.535 924 × E -1
pound-mass-foot^2 (moment of inertia)	kilogram-meter^2 (kg/m^2)	4.214 011 × E -2
pound-mass foot^3	kilogram/meter^3 (kg/m^3)	1.601 845 × E +1
rad (radiation dose absorbed)	Gray (Gy)†	1.000 000 × E -2
roentgen	coulomb/kilogram (C/kg)	2.579 760 × E -4
shake	second (s)	1.000 000 × E -8
slug	kilogram (kg)	1.459 390 × E +1
torr (mm Hg, 0°C)	kilo pascal (kPa)	1.333 22 × E -1

*The becquerel (Bq) is the SI unit of radioactivity; 1 Bq = 1 event/s.

†The Gray (Gy) is the SI unit of absorbed radiation.

1 BACKGROUND

During the past 20 years, computer codes for the prediction of shock-wave propagation in solids have become increasingly complex and sophisticated, as have experimental techniques for the measurement of shock-wave propagation. In the early 1950s the fundamental assumption of the computational models was that solid behavior could be treated as hydrodynamic--i.e., material strength effects were not important in the high-stress region.

The essential input data for the computations were obtained by rear-surface measurements of shock velocity and free surface velocity of a material in laboratory shock-wave experiments. With the aid of a few assumptions and the application of the conservation laws, each pair of shock-velocity/free-surface velocity points maps onto a point in the pressure-volume plane. The locus of states in the pressure-volume plane (or the equivalent pressure-particle velocity plane) that can be reached by shock compression of a material (from a given initial state) is called the Hugoniot equation of state, or simply, the Hugoniot.

By the early 1960s, the inadequacy of the hydrodynamic model had been conclusively demonstrated by the results of well-designed one-dimensional shock-wave propagation experiments on metals; the hydrodynamic model predicted very much lower attenuation rates than were observed. With the development of improved stress-wave generating techniques, higher-resolution rear-surface measurements, and most recently, in-material stress and particle velocity transducers, progressively more refined computational models could be tested. It gradually became apparent that the propagation of stress waves in a solid is a complex phenomenon that can be modeled accurately only when all of the important complexities of actual material behavior are incorporated into the model. The realization of this complexity has led to the use of the general term "stress wave" in place of "shock wave," which implies narrowly restricted material behavior.

At present, there exist a variety of computer codes capable of predicting with satisfactory accuracy the outcome of both one-dimensional and two-dimensional laboratory wave-propagation experiments with various metals. The common element in the successful predictions has been the development and incorporation into the computation of sufficiently accurate and comprehensive constitutive relations (a dynamic stress-volume-energy equation of state).

These material-specific constitutive relations quantitatively account for the effects on stress-wave propagation of detailed material response including yielding, plastic flow, work-hardening, fracture (including the stress-time dependence of the nucleation and growth of fracture), stress relaxation, Bauschinger effect, heating, and cooling. The constitutive relations are based on Hugoniot measurements, static high-pressure measurements, tests of mechanical properties at various strain rates, thermodynamic measurements and calculations, dynamic fracture experiments, elasticity theory, considerations of dislocation dynamics, and any other relevant data or theories that are needed and available.

The development of accurate constitutive relations for metals required extensive collaboration among shock-wave physicists, solid-state physicists, physical and mechanical metallurgists, computer code specialists, and others. Rapid progress became possibly only when the various specialists learned to communicate with one another.

One may presume that, at least in principle, the computational aspects of predicting the effects of nuclear explosions in geologic media are well understood. The heart of the prediction problem therefore appears to be the demonstrable inadequacy of present knowledge of constitutive relations for the geologic media of interest.

It is perhaps misleading to define the constitutive relations as a dynamic stress-volume-energy equation of state. Indeed, use of the term "constitutive relations" is one way of avoiding the implication that the states of interest are path-independent, thermodynamically equilibrated states. It might be better to state that the constitutive relations are a detailed description of the response of a material to stress waves. A bare bones set of constitutive relations for a wave propagation calculation could be constructed from a set of compression and release paths covering the stress-time range of interest.

The variety of possible compression and release paths for geologic media is illustrated in the following examples. Assume the geologic medium to be a compact monomineralic rock composed of a mineral known to undergo a phase transition at high quasi-static pressures. The equilibrium stress-volume behavior of this material is schematically depicted by the solid line in Figure 1(a); the dashed lines represent metastable compression curves for phase I and phase II. Figures 1(b), 1(c), and 1(d) depict some possible responses of this material to stress-wave compression and release.

Figure 1(b) illustrates metastable response. The compression path is the Rayleigh line connecting the initial state (σ_o, V_o) with the state (σ_1, V_1) on the metastable extension of the phase I compression curve. The release path is the phase I isentrope. This type of response is experimentally observed for quartz single crystals and for compact quartzite loaded to peak stresses within the stability field of coesite.[1]

Figure 1(c) illustrates rapid (somewhat overdriven) phase transition behavior. A double shock forms in the material; the compression path is from the initial state (σ_p, V_o) to a state (σ_2, V_2) on the metastable extension of the compression curve of phase I and, in the second shock, from (σ_2, V_2) to the state (σ_3, V_3) on the compression curve of phase II.

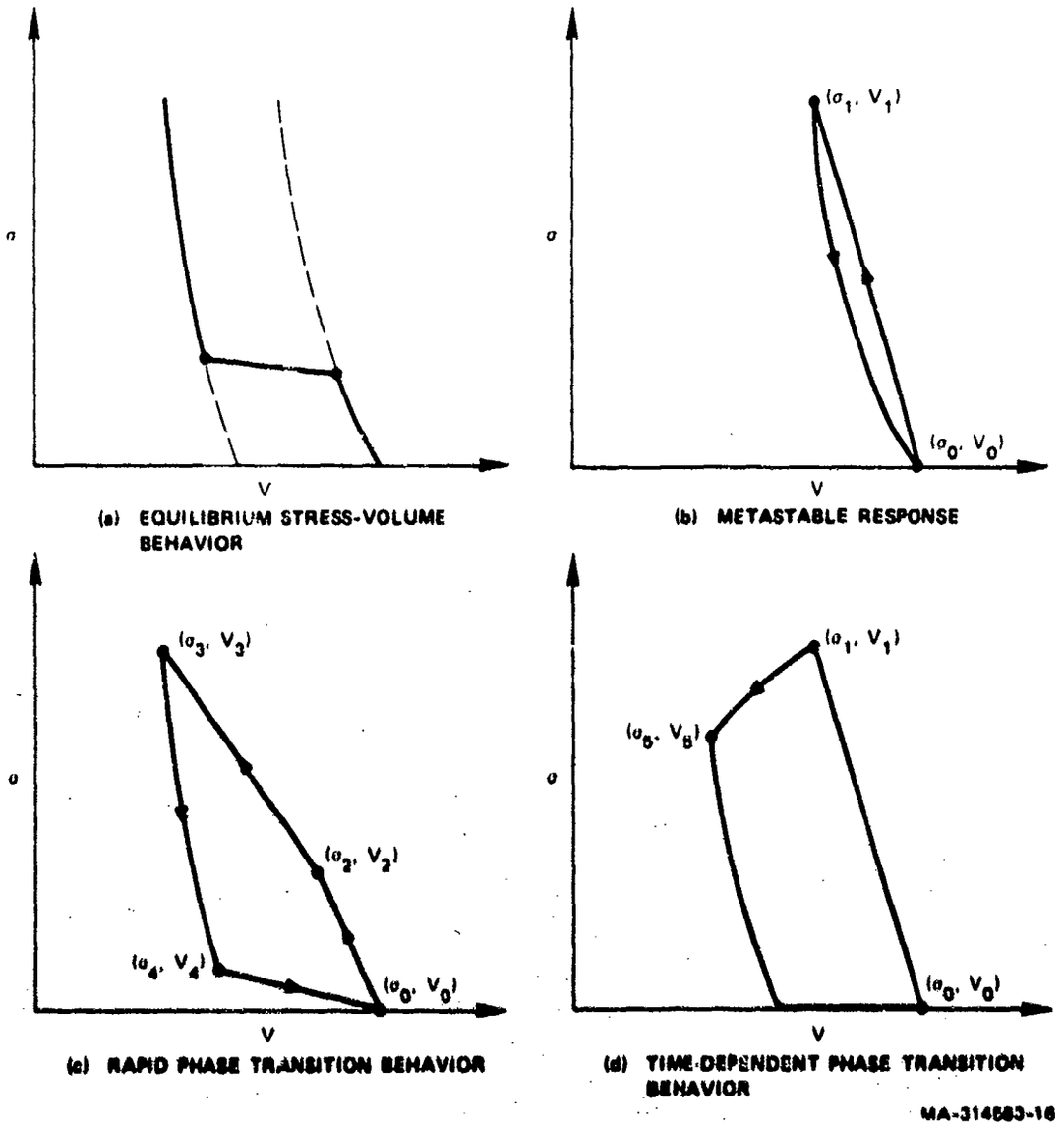

(a) EQUILIBRIUM STRESS-VOLUME BEHAVIOR

(b) METASTABLE RESPONSE

(c) RAPID PHASE TRANSITION BEHAVIOR

(d) TIME-DEPENDENT PHASE TRANSITION BEHAVIOR

MA-314583-16

FIGURE 1 EXAMPLES OF POSSIBLE COMPRESSION AND RELEASE PATHS

The release path is along the isentrope of phase II down to a state (σ_4, V_4) in the stability field of phase I and thence to the initial state. This general type of behavior has recently been observed for quartzite and feldspar loaded to peak stresses of about 50 GPa.[2]

Figure 1(d) illustrates time-dependent phase transition behavior in response to a stress pulse of relatively long duration--e.g., 10^{-3} sec. The initial compression path is to the state (σ_1, V_1) on the metastable compression curve of phase I. As the transformation proceeds, the material relaxes towards the state (σ_5, V_5) on the compression curve of phase II. The stress is relieved and the material expands along the isentrope of phase II down to zero stress before transforming back to phase I. There is a hint of this general type of behavior, on a microsecond time scale, in recent Lagrangian gage measurements of the response of dolomite.[3] However, one can argue that this type of behavior should be fairly common on a millisecond time scale at high stresses (and concomitant high temperatures), invoking extrapolations of sparse static high-pressure phase-transition-rate data.

The three examples, Figure 1(b), (c), and (d), of material response were presented in order of their effect on stress-wave attenuation. If one recalls that the area enclosed by the compression and release paths is the internal energy increase of the material, one need not invoke the details of rarefaction wave propagation to realize that the stress wave would be much more attenuated by a material responding as in Figure 1(d) than by a material responding as in Figure 1(b).

Present constitutive models of silicate behavior at high stresses are based largely on Hugoniot data derived from rear-surface measurements made over the past 20 years. Rear-surface measurements are subject to large experimental uncertainties and ambiguities of interpretation if the material response is complicated by phase transitions. These

limitations of rear-surface measurements have been largely circumvented by the recent development of in-material gages to measure stress and particle velocity. Lagrangian analysis of properly designed in-material gage experiments permits determination of complete compression and release paths, even for a material that undergoes dynamic phase transitions. In contrast to rear-surface measurements, Lagrangian analysis of in-material gage experiments does not require any assumptions of material response or of steady wave behavior, although one does require suitable stress and/or particle velocity gages.

Prior to the present work, experiments with in-material stress gages were limited to the region below 50 GPa and calibration data were available only for the region below 40 GPa. One of the objectives of the research presented here was to develop and calibrate a technique for the measurement of stress-wave profiles over the range to 100 GPa. This objective has been achieved, with the extension of the range of the manganin stress transducer to approximately 125 GPa. Using a Lagrangian array of in-material gages, we have measured the phase transition behavior of granite at a peak shock stress of 80 GPa. Tentatively, we infer that previous Hugoniot measurements do not accurately describe the respone of granite in the stress region above about 50 GPa.

II THE MANGANIN PIEZORESISTANT DYNAMIC STRESS TRANSDUCER

Review of Earlier Work--Calibrations to 40 GPa

Manganin, an alloy nominally of 84% Cu, 12% Mn, and 4% Ni, was first used as a hydrostatic pressure transducer by Bridgman in 1911.[4] It must be noted, however, that Bridgman credits Lissel with the first accurate measurements of the piezoresistivity of manganin and with the suggestion that manganin be used as a pressure transducer.[5] In 1962, Fuller and Price reported measurements of the dynamic piezoresistance of manganin,[6] and in 1964, Bernstein and Keough[7] reported on their development of the manganin dynamic stress transducer. Since that time, manganin gages have become widely used, both as in-material gages and as rear-surface gages, to instrument stress-wave experiments.

As an in-material gage, the manganin transducer is imbedded in the material under investigation. Insulation layers, necessary if the material is an electrical conductor, are made as thin as possible in order to permit the transducer to rapidly achieve stress equilibrium with the material. The rear-surface gage consists of a manganin transducer imbedded in an insulator of known shock properties. This gage is bonded to the rear surface of the material under investigation. The stress response of this material is inferred from measurements of the stress wave transmitted into the insulator.

It has been stated that the reproducibility of manganin stress-wave measurements is about 20%;[8] this statement was apparently based on the disagreement between the Fuller and Price results and the Bernstein and Keough results. However, one must recognize that accuracy was not a prime consideration in some of the exploratory studies of the dynamic response of manganin. More recent results indicate that the dynamic piezoresistance of manganin is highly reproducible and that interlaboratory agreement is excellent, at least over the carefully studied stress range of 2 to 15 GPa.

Over the stress range of 2 to 15 GPa, Barsis et al.[9] measured a dynamic piezoresistance coefficient for manganin of 2.9%/GPa. Stresses were produced by plate impact, resulting in flat-topped stress waves, and their claim of 1% accuracy in stress measurement appears justified. Their gages were 50-ohm grids, chemically milled from Driver-Harris shunt manganin foil (10 wt% Mn, 3.5 wt% Ni, balance Cu). The gages had a sufficiently high resistance to permit accurate two-terminal measurements, and their measurement technique (the gage formed one leg of a Wheatstone bridge) cannot be faulted. They do not so state, but one may infer from their paper that the reproducibility of their stress-resistance values was within about ± 3%. Over the stress range of 0 to 2 GPa, their data indicate that the dynamic piezoresistance coefficient increases from about 2.4%/GPa (the hydrostatic value) to 2.9%/GPa.

Lee[10] has also made accurate measurements of the piezoresistance of manganin over the stress range of 0 to 10 GPa. His measurements were made on 1-ohm four-terminal gages made from Driver-Harris wire (12 wt%, Mn, 4 wt% Ni, balance Cu) imbedded in epoxy. Despite differences in gage construction, manganin composition, and measurement techniques, Lee's results were virtually identical with those obtained by Barsis et al. Lee's stress measurements (of flat-topped stress waves) appear to have been accurate to within 1%, and his relative resistance measurements were apparently of similar accuracy, except at stresses below 2 GPa, where one may infer possible errors of 5%. Lee fitted his data with a cumbersome fourth-order polynomial that is valid only over the range of 0 to 10 GPa. Over the range of 2 to 10 GPa, however, his data fit a linear coefficient of 2.9%/GPa.

Fuller and Price[8] initially reported a much lower dynamic coefficient of 2.1%/GPa for two-terminal 3-ohm wire gages in epoxy. On the basis of improved Hugoniot data for the epoxy, they subsequently revised the coefficient upward to about 2.4%/GPa.[11] However, they used explosive-in-

contact geometries to produce triangular, rapidly attenuating stress waves and inferred stress from shock velocity measurements. Unless adequate corrections are made for attenuation, this procedure leads to an overestimate of stress. One may infer that errors in stress measurement, together with errors in two-terminal resistance measurement, are adequate to account for the discrepancy between their results and more recent results.

Keough and his co-workers have made numerous four-terminal measurements of the dynamic piezoresistance of manganin in various insulators over the stress range of 0 to 36 GPa.[12,13] They found no essential differences between the response of wire gages (12 wt% Mn) and the response of gages photoetched from shunt manganin foil (10 wt% Mn) at stresses above the insulator Hugoniot elastic limit (HEL). At stresses below the insulator HEL, wire gages in Lucalox (fully dense Al_2O_3 ceramic) had an anomalously high resistance change, relative to foil results, that was attributed to the effects of wire deformation. Keough fitted his data to a coefficient of 2.9%/GPa over the range of 0 to 17 GPa. He interpreted his higher-stress data in terms of a decrease in the differential piezoresistance coefficient to about 1.8 %/GPa over the stress range between 17 and 36 GPa. Keough used both plate-impact (flat-topped stress waves) and explosive-in-contact (triangular stress waves) in his calibration experiments, and the accuracy of his stress measurements ranged from about 1% for the best plate-impact experiments to about 10% for some of the explosive-in-contact experiments. It should be noted that Keough did not make extensive measurements in the stress range below 2 GPa; he simply extrapolated his higher stress results downward. At least over the range of 2 to 15 GPa, the results of Keough and coworkers appear confirmed by the subsequent studies of Lee and of Barsis et al. The scatter in Keough's results is largely ascribable to errors in stress measurement and to uncertainties in the insulator Hugoniots.

The piezoresistance of manganin has been less intensively studied in the stress range obove 15 GPa. Possible errors in the Fuller and Price studies, which extend to 30 GPa, have already been noted. Dremin and Kanel[14] made two-terminal measurements of the response of 1-ohm manganin gages over the stress range of 10 to 45 GPa. They do not estimate the accuracy of their measurements; one may infer possible 10% errors in stress determination inherent in their use of "standard" explosive-in-contact geometries.

Lyle et al.[15] measured the dynamic piezoresistance of manganin in six experiments, over the range of 7.7 to 39 GPa. Their stress determinations, based on flat-plate impact velocities, are inferred to have been accurate to within at least 2%. However, their two-terminal resistance measurements of 7-ohm gages may have been of lower accuracy. Their data for the experiments at stresses below 17 GPa imply a piezoresistance coefficient of 2.7%/GPa, which is significantly less than the value of 2.9%/GPa cited above. Their data above 17 GPa progressively diverge from Keough's results, although they do support Keough's inference of a decrease in the differential piezoresistive coefficient of manganin. Lyle et al. measured a resistance increase of 98% at 39.2 GPa; if one extrapolates Keough's calibration from 36 GPa, a 98% resistance increase would correspond to a stress of about 46 GPa. It must be noted that most of Keough's measurements above 17 GPa were exploratory in nature; accuracy of stress determination was not a prime consideration. On the other hand, the major uncertainty in the Lyle et al. two-terminal measurements is the change in lead resistance at high shock stresses. At 40 GPa, the calculated Hugoniot temperature of their copper leads is about 300°C, corresponding to a doubling of the 20°C initial lead resistance. One would expect an additional increment in lead resistance due to lattice defects generated in shock compression, and further changes in lead resistance would be caused by lead stretching due to divergent flow where the leads exit the high-stress region.

It must be noted that the dynamic calibrations of manganin are based on the response of manganin to a peak stress and are not necessarily relevant to the response of manganin upon subsequent stress release. Keough has noted an apparent hysteresis in the unloading piezoresistive response of manganin; the final resistance of a gage after a loading-unloading cycle is higher than the initial resistance. The magnitude of this "permanent" resistance increase ranged from 2% of the initial resistance after a 0-to-6-to-0 GPa cycle to about 7% after a 0-to-15-to-0 GPa cycle. Limited calibration data obtained in step-release experiments, however, indicated that the piezoresistive behavior of manganin during release appears to be linear. Barsis et al. also noted that their gages failed to return to initial resistance values after stress release, and suggested that mechanical damage was the cause.

Barsis et al.[9] and Rosenberg et al.[16] have observed that the dynamic piezoresistance of manganin is significantly decreased by prior cold work (50% reduction in thickness by rolling). Rosenberg et al. also noted that the hysteresis is decreased as a result of the cold work. Both groups found that the original piezoresistance was regained by annealing.

Present Work--Calibration to 125 GPa, (1250 kbar) and Unloading Data

The material used in the present study was 0.001-inch-thick (0.025 mm) manganin foil shunt stock from the Driver-Harris Company, Harrison, New Jersey. This material has a nominal composition of 86% Cu, 10% Mn, 4% Ni, and is from the same roll as the material studied by Keough and Wong. All measurements were made with four-terminal gages having aspect ratios (width-to-thickness) of at least 20:1 in order to minimize possible two-dimensional flow effects. The gage is bonded between plates of insulating material to form a gage package that is bonded to the rear surface of a metal base plate.

It must be noted that the details of manganin gage construction and packaging are crucial to successful operation in the stress range above about 45 GPa. Many of the insulators commonly used in gage package construction become fairly good electrical conductors at very high shock stresses. The gage package design that evolved in the course of the present study is illustrated in Figure 2. The manganin gage element is bonded between plates of a material known to remain a good insulator at high shock stresses. Fully dense Al_2O_3 ceramics and fused silica were found to meet this requirement. The insulators and gage element must be bonded; elimination of trapped air that would ionize under shock compression is more important than mechanical strength. After some experimentation, we adopted a standard bonding medium of type 1100 Homalite epoxy, loaded with 31 wt% 0.3-μm α-Al_2O_3 powder. The Al_2O_3 loading appears to result in a somewhat higher resistivity, relative to unloaded epoxy, at high shock stresses, but it must be emphasized that the resistivity of even the loaded epoxy becomes quite low, of the order of one ohm-cm, at shock stresses near 100 GPa. Therefore it is important to minimize the area of the shunt path through the loaded epoxy by making the bond layer as thin as possible. Typical bond layer thicknesses achieved were 0.033 mm, including the 0.025-mm-thick gage element. (The 31 wt% loading of Al_2O_3 was the highest loading compatible with minimum bond-layer thickness.) The length of the shunt path through the epoxy is maximized by the geometry of the gage element, and the relative effect of shunting is reduced by using gages of very-low-impedance.

A flat-topped shock wave is produced by the impact of an explosively accelerated metal flyer plate on the base plate. Since the Hugoniots of the flyer-plate material and the base-plate material are known, the shock stress in the base plate can be determined by a single measurement, either of flyer-plate impact velocity, of shock velocity in the base plate, or of free surface velocity of the base plate. In most of the

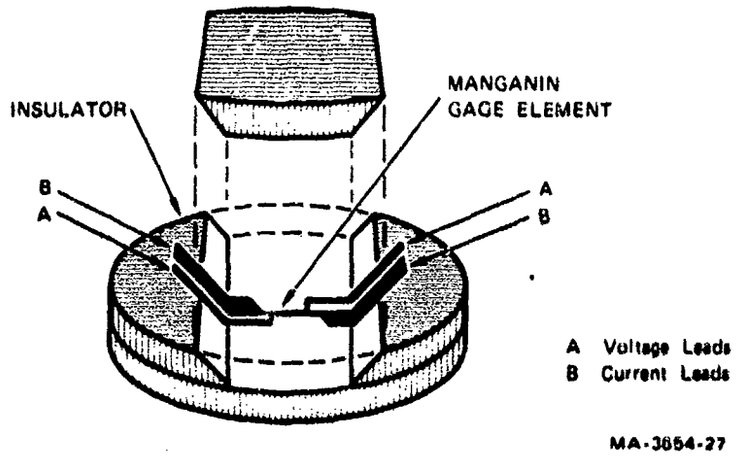

FIGURE 2 MANGANIN GAGE PACKAGE DESIGN

present experiments, coaxial self-shorting pins were used to measure all three quantities and to measure the planarity of flyer-plate impact. In general, these three independent measurements of base-plate stress agreed within 5% or better. In a few experiments, because of either oscilloscope malfunction or a faulty pin, only free-surface-velocity measurements were obtained. For these experiments our worst-case estimate of the accuracy of base-plate stress measurement is ± 10%.

The stress in the manganin gage package is determined by impedance matching at the base-plate gage-package interface, using available Hugoniot data. With one exception, a fused silica gage package, Vistal* (a fully dense Al_2O_3 ceramic) was used as the gage package material in the calibration experiments.

Although no Hugoniot measurements have been reported for Vistal, per se, one may note that Hugoniot measurements have been reported for single-crystal Al_2O_3 and for various Al_2O_3 ceramics over the stress range of present interest. Since the single-crystal data and ceramic data are identical within experimental error (in the pressure-volume plane), we feel safe in presuming that the single-crystal Hugoniot adequately represents the Vistal Hugoniot.

The base-plate materials used were OFHC copper and 2024 T-6 aluminum, chosen because their Hugoniots are very well determined. The release adiabat of copper was assumed to be identical with the Hugoniot, in order to calculate the stress transmitted into Vistal or fused-quartz gage packages. Experimental data on copper free-surface velocities indicate that, at worst, this assumption would lead to only a 2% error in calculated gage package stress. In calculating the stress transmitted into Vistal from an aluminum base plate, we approximated the reflected shock Hugoniot of aluminum by the single shock Hugoniot. Calculations

*Coors Corp., Golden, Colo.

of internal energy differences between reflected shock states and single shock states in aluminum, together with available P-V-E equation-of-state data obtained from shock experiments with porous Al samples, indicate that this approximation introduces an error of less than 2% in calculated stress.

In some experiments, the gage packages were backed by a lower-impedance material to provide a step release to an intermediate stress, calculated by assuming the release adiabat of the gage package material to be identical with its Hugoniot. Since Al_2O_3 is relatively incompressible and is experimentally found to undergo no phase transitions over the stress range of interest, this assumption is reasonable for Vistal gage packages. Fused quartz is highly compressible and is believed to undergo a phase transition; the release adiabat is expected to differ significantly from the Hugoniot. In the absence of accurate experimental data, we can only bracket the range of possible fused-quartz release adiabats by extreme assumptions of material behavior during release.

The measurement system used was essentially identical with the system used by Keough and Wong. A constant current is passed through the four-terminal manganin gage and the voltage across the central portion between the voltage leads is monitored by a camera-equipped oscilloscope. The power supply consists basically of a 90-μF capacitor (charged to 500 V) in series with a ballast resistor, a silicon-controlled rectifier (SCR) switch, and the gage. In an experimental measurement, the power supply is triggered 5 to 50 μs prior to shock-wave arrival at the gage. The initial current step through the gage is recorded as a voltage step, proportional to the gage resistance. The change in gage resistance upon shock wave arrival appears as an additional voltage step on the oscilloscope record. The ratio of resistance change ΔR to initial resistance R_o can be determined from the measured voltage ratio $\Delta V/V_o$, corrected for the effects of changing lead and gage resistances

and for any decay of capacitor voltage over the period of measurement. In the present experiments these corrections amount to less than 1% and can be ignored.

Ideally, the voltage ratio $\Delta V/V_o$ (and therefore the resistance ratio $\Delta R/R_o$) can be determined to an accuracy of about 1%, limited primarily by oscilloscope linearity. Because of the exploratory nature of the present experiments, optimal instrumentation conditions were not predictable, and the accuracy of $\Delta V/V_o$ measurement was somewhat lower, but generally within about 3%.

The major source of error and the major problem associated with the use of manganin gages at very high shock stresses is shunting caused by the development of substantial electrical conductivity in shock-compressed insulators. In the present work we have attempted to minimize the shunting effect by careful attention to gage geometry and construction and by using gages of very low impedance (0.15 ohm). This is contrasted with the usual practice of using 1-to 10-ohm gages in four-terminal measurements and 10-to-50-ohm gages in two-terminal measurements.

A near-ideal gage record (0.15-ohm gage in Vistal) at 80 ± 2 GPa is reproduced in Figure 3. The voltage-versus-time profile corresponds in shape and duration to the stress-versus-time profile calculated from the flyer-plate impact parameters. Figures 4,5,6 and 7 are gage records of flat-topped 100-GPa stress waves, showing the effects of progressive improvements in gage design. The 1.5-ohm-gage record (Figure 4) is virtually useless except as an indication of stress-wave time of arrival. Reduction of gage impedance to 0.15 ohm (Figure 5) resulted in a substantial improvement. Although the gage profile is not flat-topped, the droop could be interpreted as the result of the progressive increase in the area of the shunt path as the shock propagated through the gage package.

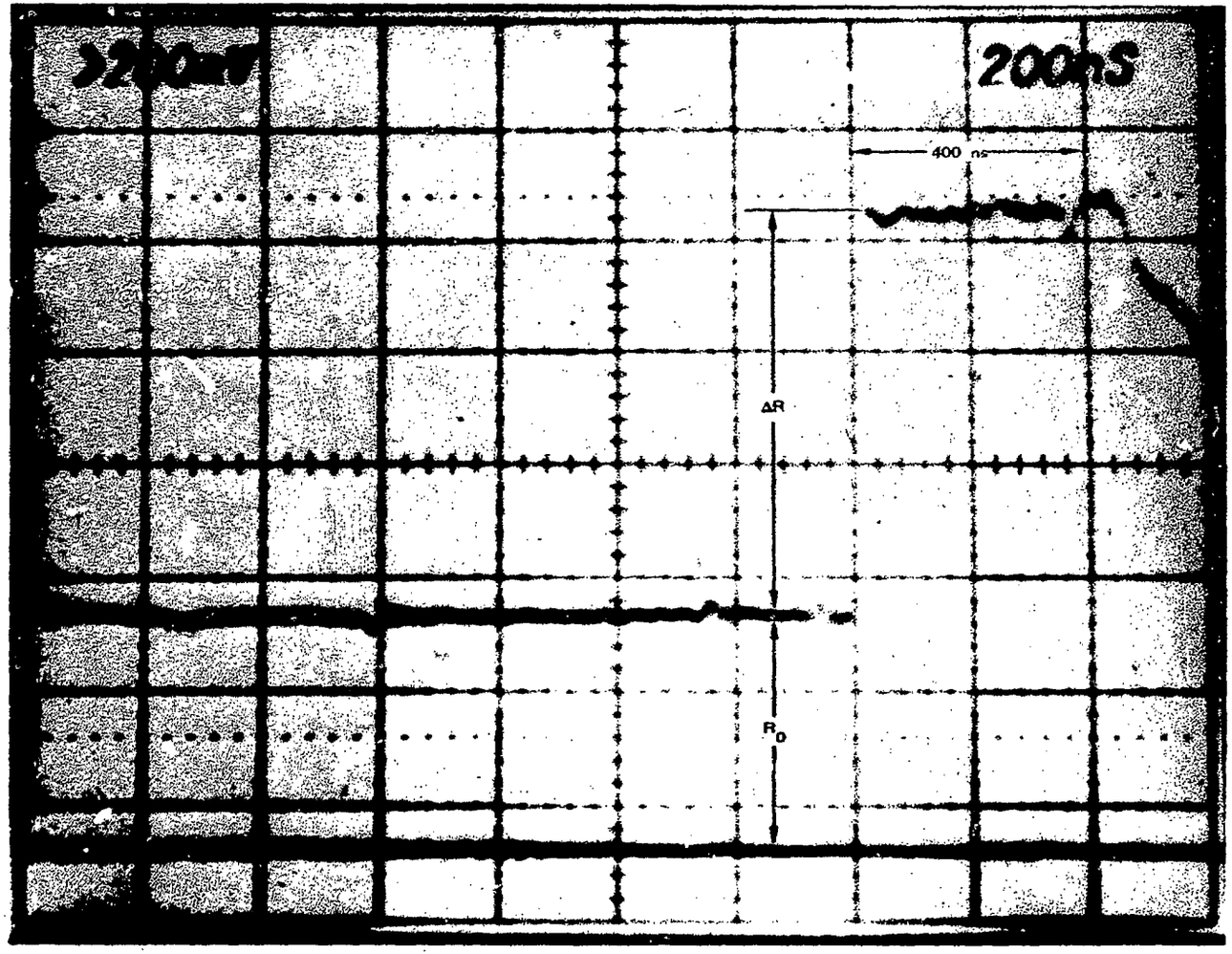

MP-3654-3

FIGURE 3 MANGANIN GAGE RECORD AT 80 ±2 GPa

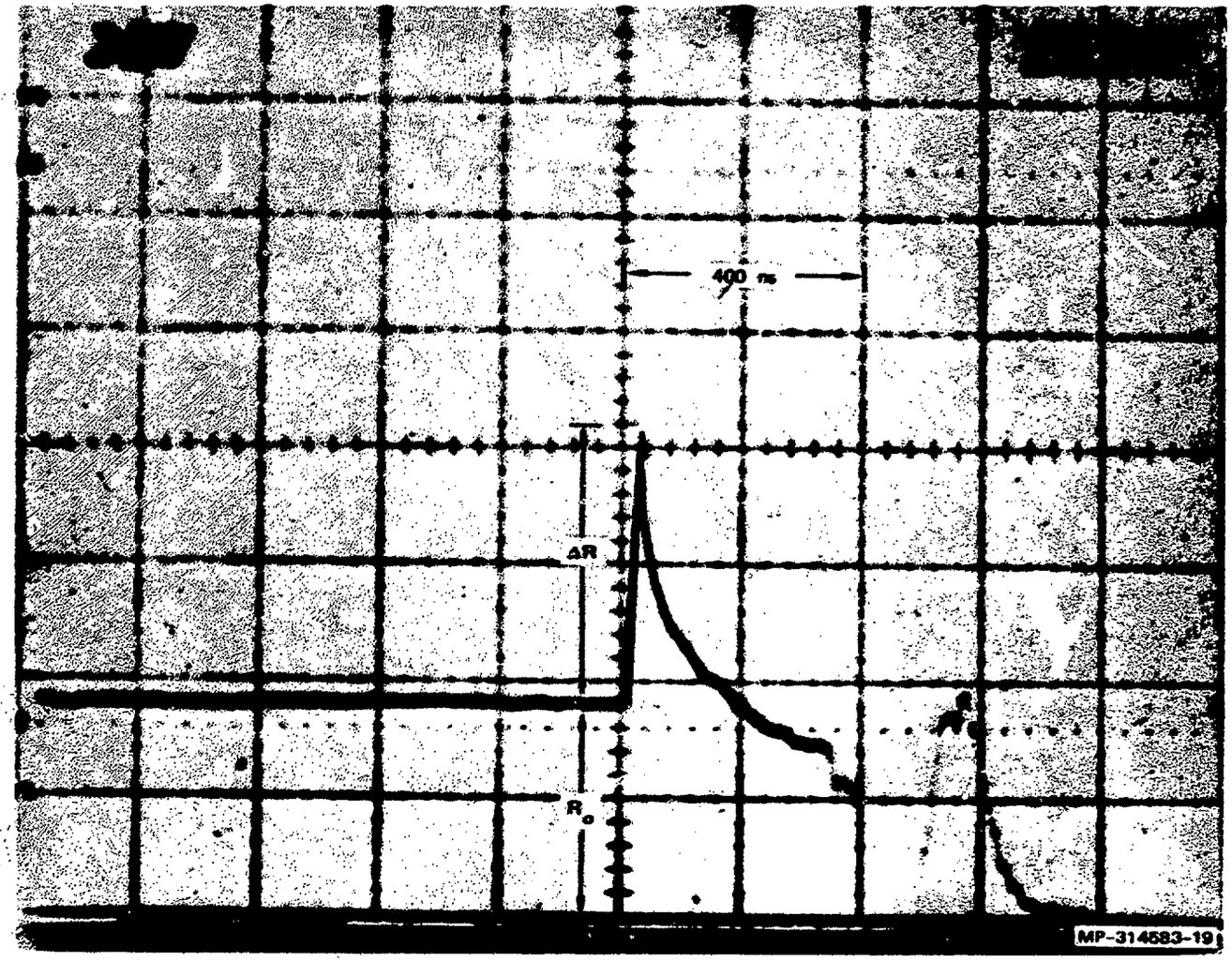

FIGURE 4 RECORD OF 1.5-ohm MANGANIN GAGE IN EPOXY-BONDED LUCALOX AT 100-GPa PEAK STRESS

(Initial rise and fall of record darkened for clarity in this reproduction)

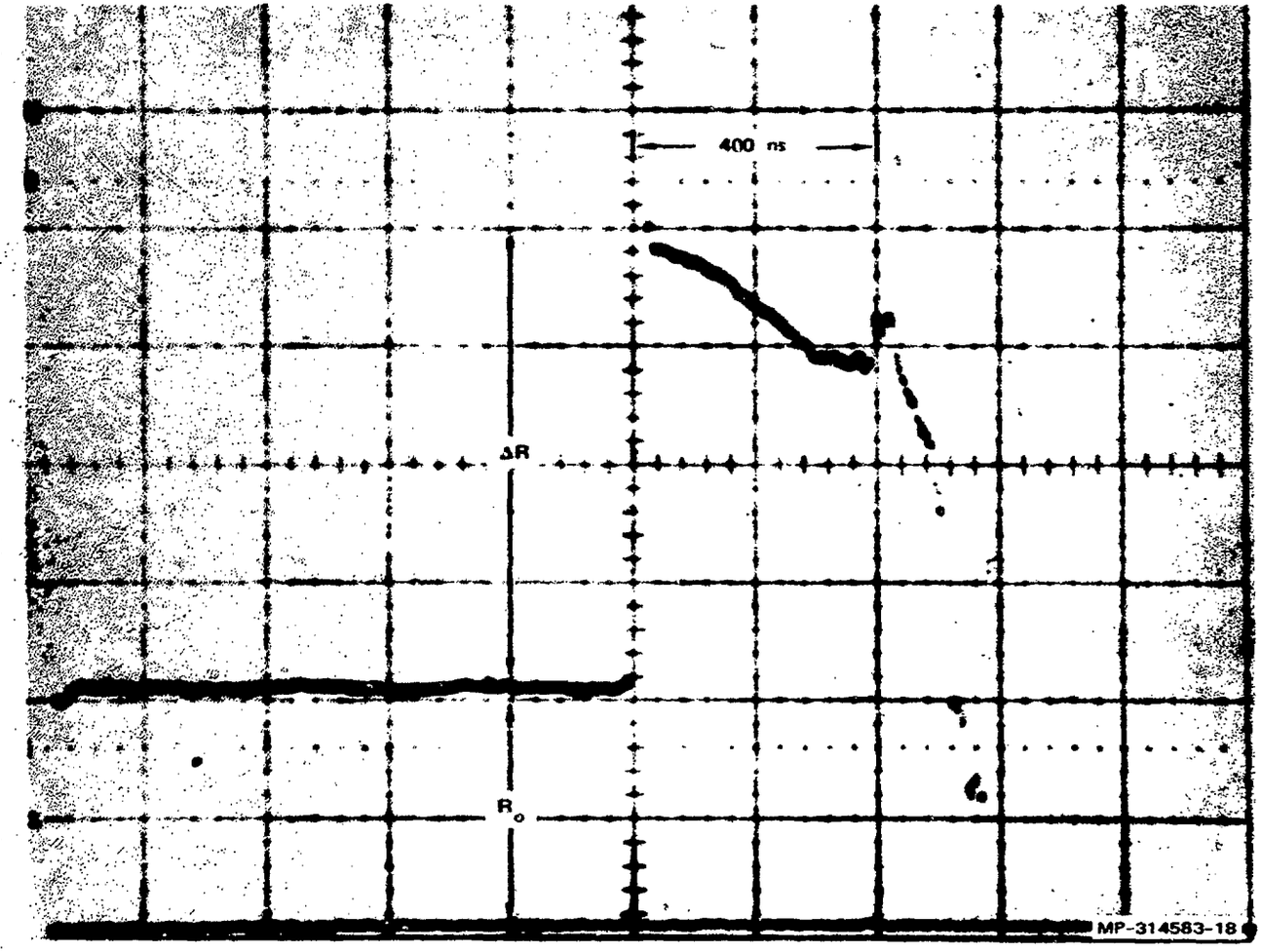

FIGURE 5 **RECORD OF 0.15-ohm MANGANIN GAGE IN EPOXY-BONDED LUCALOX AT 100-GPa PEAK STRESS**

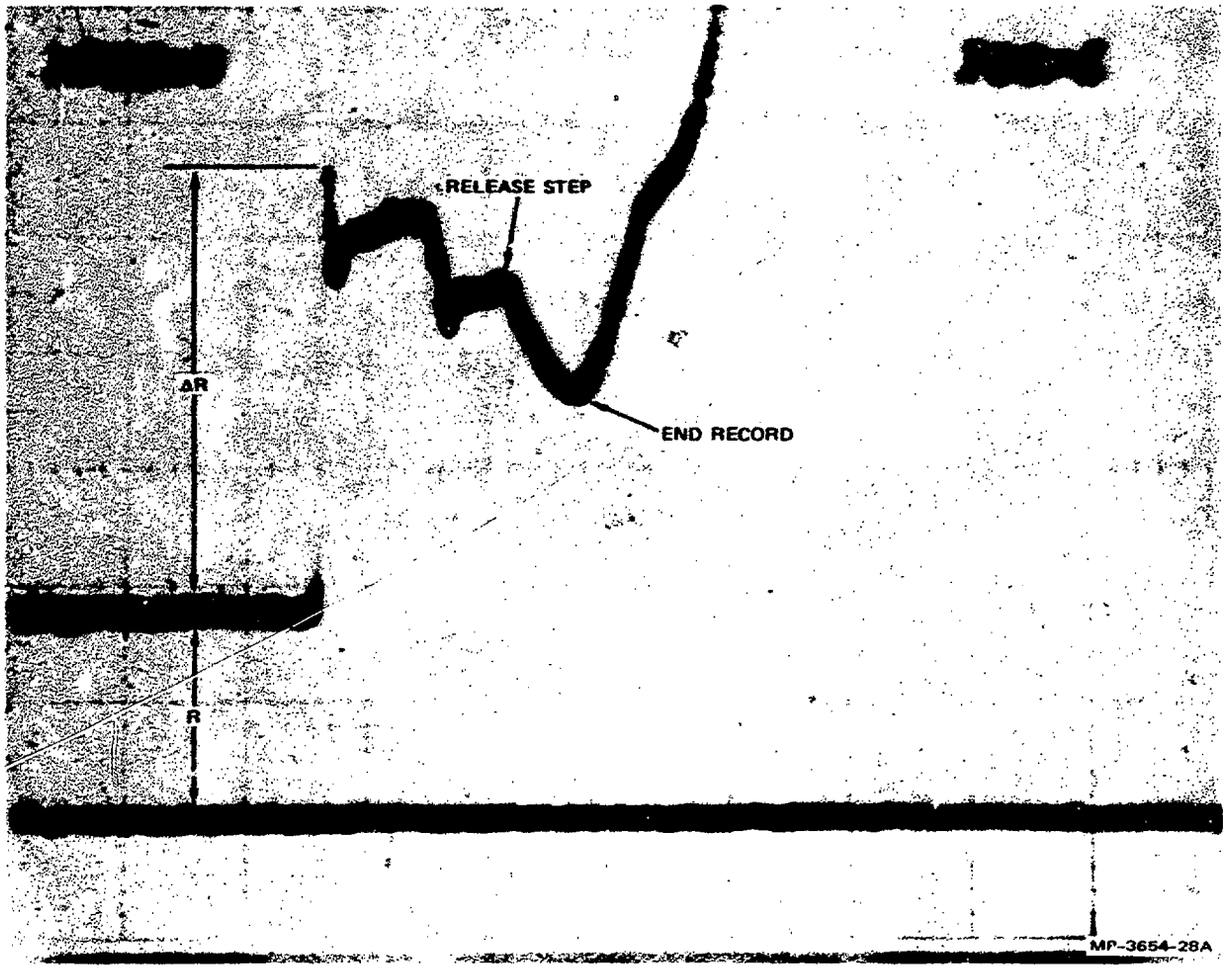

FIGURE 6 RECORD OF IMPROVED-GEOMETRY 0.15-ohm MANGANIN GAGE AT 100 GPa, WITH RELEASE TO 71 GPa

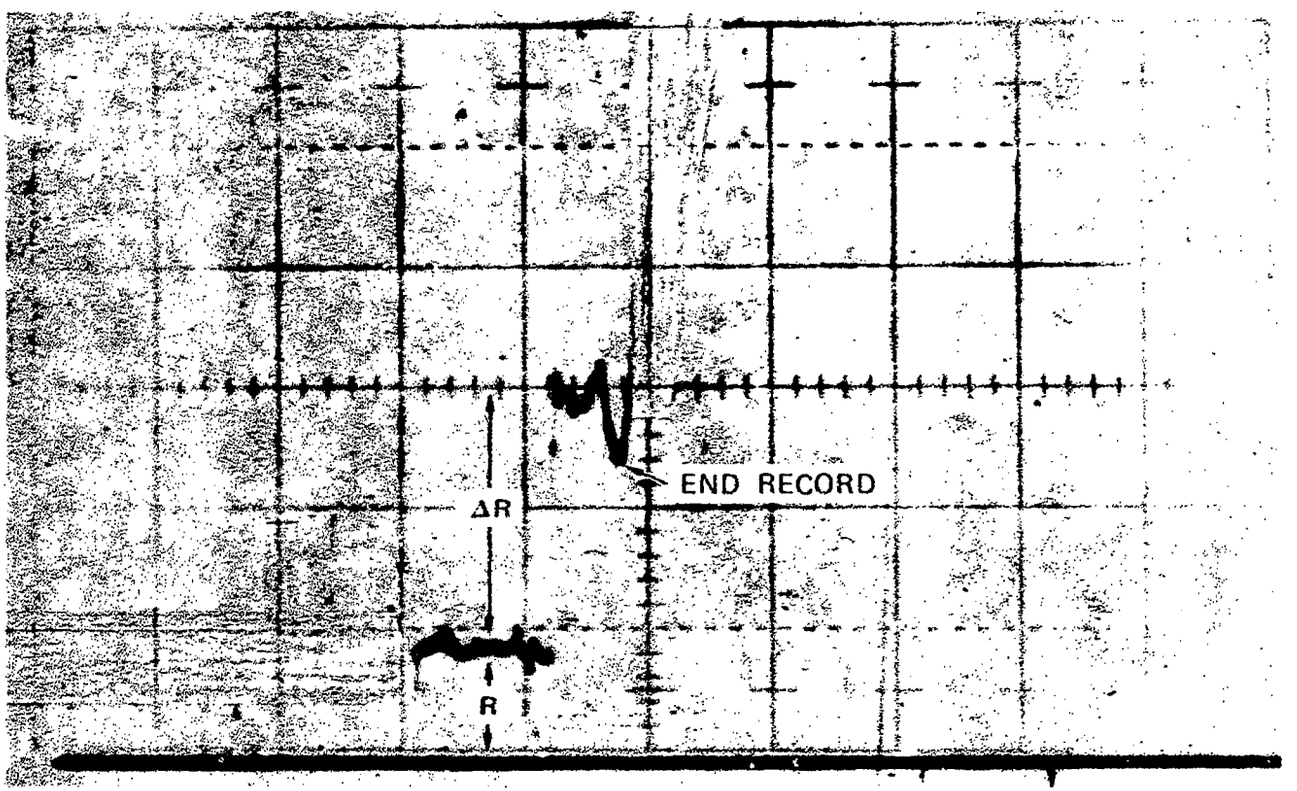

MP-3654-29

FIGURE 7 RECORD OF 0.05-ohm MANGANIN GAGE AT 100 GPa

Figure 6 illustrates the results of improvements in gage geometry and construction, with a 0.15-ohm gage of the type used in most of the present calibration experiments, as illustrated in Figure 2. Another difference in the gages of Figures 4 and 5 was the use of Vistal instead of Lucalox as the gage package material. However, since the two materials are similar, fully dense, Al_2O_3 ceramics differing only in grain size, one would not expect them to differ significantly in electrical conductivity at high shock stresses. The gage package of Figure 6 was backed by aluminum in order to obtain a step release to approximately 71 GPa. The correspondence between the observed voltage-versus-time profile and the predicted stress-versus-time profile is greatly improved, in comparison with the record of Figure 5. The presence of the spike on stress-wave arrival and the deviation from flatness of both the stress peak and the release step are evidence that shunting has not been completely eliminated.

Further improvement in the fidelity of the manganin gage response was attempted via reduction of gage impedance to 0.05 ohm (Figure 7). Although this record is noisy, one can observe that the relative resistance change is about 10% larger than was observed with the 0.15-ohm gage at the same stress of 100 GPa. One may deduce from the shape of the peak that shunting similar in character to that of Figure 6 is still present.

Since the 0.15-ohm and 0.05-ohm gages were geometrically similar, one can calculate an average resistance of about 10 ohms for the shunt path through the insulator at 100 GPa. Since the gage current leads are manganin and since they also change resistance upon shock arrival, it is appropriate to base this calculation on the two-terminal resistance of the gage, measured across the current-carrying region in the gage plane. These values are 0.4 ohm (for the 0.15-ohm gage) and 0.1 ohm (for the 0.05-ohm gage).

The results of the calibration experiments are listed in Table 1. The raw resistance ratios are based on measurements of the flat portion of the voltage peak, and we also include the ratio determined from the height of the initial spike, where present. In one experiment, a gap in the oscilloscope trace is noted. It is presumed that the gap was due to a voltage excursion (an initial spike) that exceeded the recording capability of the oscilloscope camera. The corrected resistance ratios listed in Table 1 reflect estimates of both measurement errors and the magnitude of the shunting correction for each experiment. In estimating the shunting correction, we have taken into account the presence and amplitude of initial spikes, the correction at 100 GPa inferred from experiments with gages of different impedance, and the correspondence between observed voltage-versus-time records and calculated stress-versus-time profiles.

The present results, some of Keough's higher-stress data, the 2-to-15-GPa calibration line, and the results of Lyle et al. are plotted in Figure 8. Over the stress range of 15-to-125 GPa, the response of manganin appears to be linear, within the accuracy of the experiments, and both loading and unloading data can be fitted by a piezoresistance coefficient (over the stated range) of about 2.1% ($\pm$ 0.2)/GPa. If one excludes the apparently complex region below 2 GPa, all of the reliable data on the dynamic piezoresistance of manganin can be adequately fitted by the two-piece linear calibration curve:

$$P = \begin{cases} 35\ \text{GPa}\ (\Delta R/R_o), & 2\ \text{GPA} \le P \le 15\ \text{GPa} \\ 48\ \text{GPa}\ (\Delta R/R_o) - 5.6\ \text{GPa}, & P \ge 15\ \text{GPa}\ . \end{cases}$$

The data of Barsis et al. and of Lee on the response of manganin below 2 GPa can then be adequately fitted by a second-order polynomial:

$$P = 42\ \text{GPa}\ (\Delta R/R_o) - 120\ \text{GPa}\ (\Delta R/R_o)^2, \quad P < 2\ \text{GPa}\ .$$

Table 1
MANGANIN GAGE CALIBRATION RESULTS

Shot No.	Gage Package Material	Loading Calibration			Release Calibration			
		Stress (GPa)	R/R_o Observed	R/R_o, Estimated Corrections Made	Backing Material	Stress (GPa)	R/R_o, Observed	R/R_o, Corrected
3654-1-4	Fused silica	32.5 ± 1	0.74	0.74-0.76	PMMA	25 ± 3	0.6	0.58-0.62
					Air	0	0	0-0.05
3654-1-4	Vistal	80 ± 2	1.7	1.7 -1.8	Al	55 ± 1	1.2-1.3	1.2-1.3
					Air	0	0.05	0.05-0.1
3654-1-4	Vistal	80 ± 2	1.74	1.75-1.8	--	--	--	--
3654-1-8	Vistal	88 ± 7	1.8	1.8-1.9	Al	61 ± 7	1.4	1.4-1.5
3654-1-12	Vistal	100 ± 3	1.9 2.0 spike	2.2-2.4	Al	71 ± 3	1.5	1.5-1.6
3654-1-12	Vistal	100 ± 3	2.1 2.3,2.4 spikes	2.2-2.4	(0.05-ohm gage)	--	--	--
3654-1-11	Vistal	100 ± 5	1.85	2.2-2.4	Al	71 ± 5	1.4-1.5	1.5-1.7
3654-1-6	Vistal	120 ± 7	2.15 2.5 spike	2.5-2.7	Al	88 ± 7	1.9	2.0-2.2
3654-1-6	Vistal	120 ± 7	2.0 2.5 spike	2.5-2.7	Al	88 ± 7	1.9	2.0-2.2
3654-1-3	Vistal	122 ± 7	2.1 (gap in trace implies fast spike)	2.4-2.7	--	--	--	--
3654-1-5	Vistal	125 ± 5	2.2 2.35 spike	2.5-2.8	Al	92 ± 5	1.9	2.0-2.2

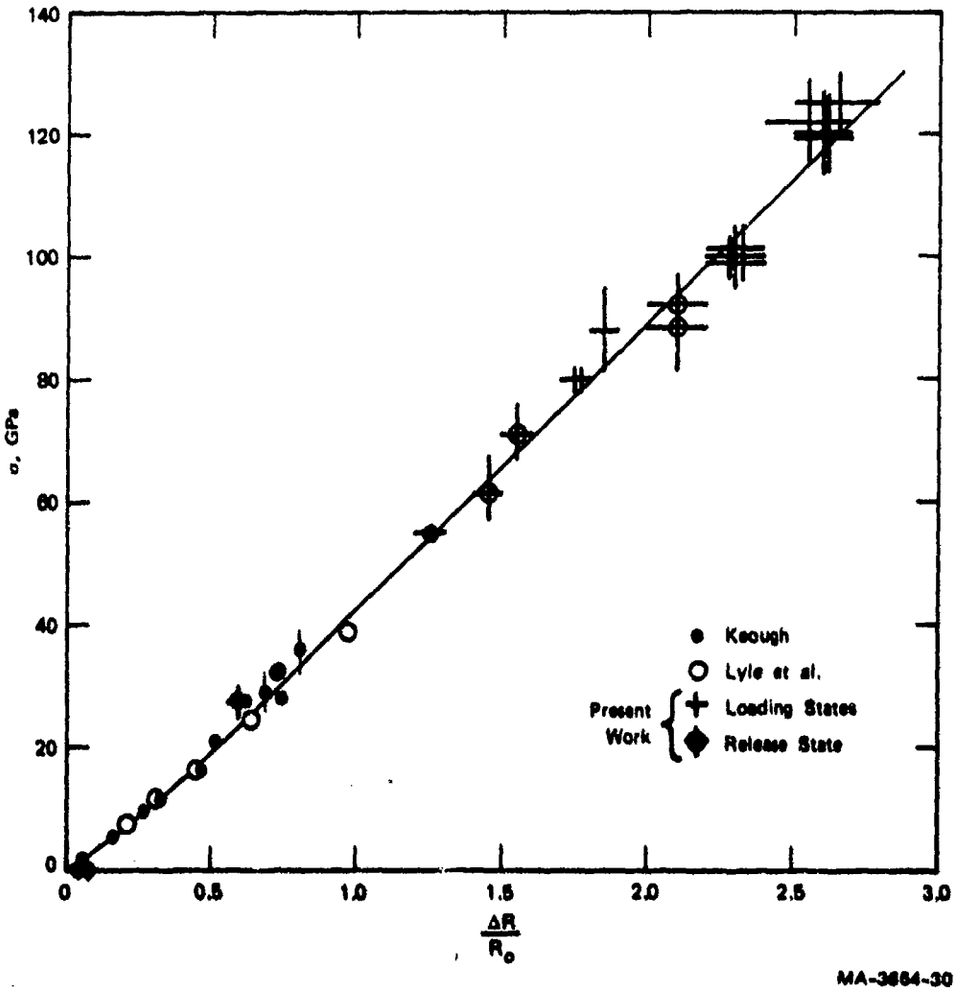

FIGURE 8 MANGANIN CALIBRATION CURVE, 0.125 GPa

For the dynamic loading regime, the accuracy of this three-piece calibration curve is estimated to be ± 5% over the range of 0 to 15 GPa, decreasing above 15 GPa to about ± 10% over the range of 30 to 125 GPa. On the basis of present evidence, the same calibration curve applies to the unloading response of manganin, with an estimated accuracy of ± 10% over the entire range and an additional constant error term of + 0 to 3 GPa. The constant error term is a reflection of the observed hysteresis, the "permanent" resistance change of a manganin gage after unloading from high dynamic stress.

Discussion

The piezoresistance of manganin appears to be remarkable well behaved over the entire dynamic stress range of 0 to 125 GPa, for both loading and unloading. Although a more accurate calibration in the high stress region would be desirable, the manganin gage is now sufficiently well developed for practical use in the study of complex phenomena such as dynamic phase transitions over the stress range to 125 GPa.

We note that Murri and his coworkers have used in-material Lagrangian arrays of manganin stress gages to obtain loading and unloading paths (in the pressure-volume plane) for quartz, feldspar, and dolomite rocks over the stress range to about 50 GPa. It now seems possible to extend the Lagrangian gage technique to much higher stresses, provided that the materials of interest do not become excessively good electrical conductors under shock compression.

In interpreting the results of very-high-stress manganin gage measurements, the greatest uncertainty is associated with the possibility of shunting due to shock-induced conductivity effects in the surrounding material. This uncertainty can be greatly reduced by using two gages, geometrically similar but differing in initial impedance by about a factor of two, in each gage plane of an in-material gage experiment. Any

difference in gage response would serve as a basis for estimating the shunting correction. It must also be noted that we interpret our successful use of 0.05-ohm manganin gages as an indication that gages of even lower initial impedance, perhaps as low as 0.005 ohm, should be tried.

III MUTUAL-INDUCTANCE PARTICLE VELOCITY GAGE

The mutual-inductance particle velocity gage has been extensively developed for use in a low-stress (0 to 2 GPa) environment. The gage is currently in laboratory use and it has been successfully used in the field in the Essex, Mixed Company, and Pre-Dice Throw programs.

The gage consists of interleaved primary and secondary windings imbedded in an insulating matrix. The primary winding is energized by a constant current prior to stress-wave arrival. On stress-wave arrival, the length of the gage changes and the mutual inductance therefore changes, with the result that a signal is generated in the secondary winding. Particle velocity u and signal voltage E are related through the equation

$$E = (M\ I/L)\ u$$

where M is the mutual inductance, I is the current in the primary, and L is the gage length.

To adapt this gage to the very-high-stress region (100 GPa), a primary requirement is that the gage be imbedded in a material that remains a reasonably good insulator at such high shock stresses. If the environment is noisy, shielding will be necessary, and it is important to determine the sensitivity of the gage to a nearby moving conductor (the shield).

A prototype gage was constructed, using a fused silica insulating matrix. Fused silica remains a good insulator up to very high shock stresses. The design is illustrated in Figure 9.

For the experiment, we used a standard aluminum gas gun projectile, modified by the addition of a 51-mm-long solid Lucite head extension to

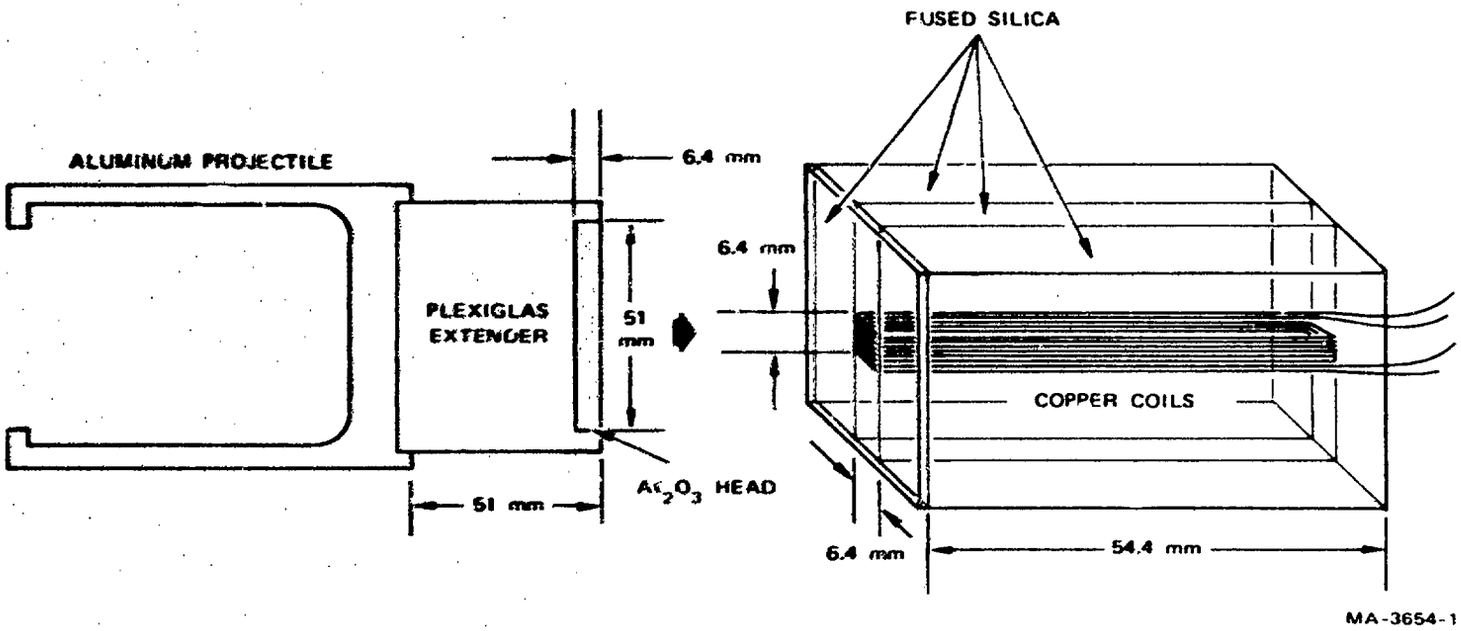

FIGURE 9 SCHEMATIC DIAGRAM OF MUTUAL INDUCTANCE PARTICLE-VELOCITY GAGE EXPERIMENT

which was attached a 6.4-mm-thick Lucalox (Al_2O_3 ceramic) head. This projectile, accelerated by maximum helium pressure (41 GPa) in the SRI 63 mm gas gun, impacted the fused silica gage package at a velocity of 0.773 km/s. Using available Hugoniot data for fused silica and for Al_2O_3 ceramic, together with the measured impact velocity, we calculated an impact stress of 7 GPa and a particle velocity in the fused silica of 0.60 km/s. Analysis of the gage record (Figure 10) yielded a peak particle velocity of 0.55 km/s, about 8% below the predicted value. Possible errors in either the prediction or the analysis of the record are large enough to account for the discrepancy.

In a previous test of this gage package we used a special nonconductive gas gun projectile because we feared that the response of the gage would be perturbed by the proximity of a rapidly moving conductor. Our failure to obtain data in that experiment was attributed to projectile breakup during acceleration. Since we did not wish to be sidetracked by problems of nonconductive projectile development, we simply added a nonconductive extension to a standard aluminum projectile for the second experiment. We did not know how long the extension had to be, to avoid perturbation of the gage response by the aluminum portion of the projectile. However, since attainable impact velocity decreases with increasing projectile mass, maximum impact velocity was a conflicting requirement. The 51-mm length chosen was a compromise value, based on experience with loop-type electromagnetic particle velocity gages. We therefore used an additional oscilloscope to monitor the gage output during projectile approach. We were able to observe no signal attributable to perturbations by the conductive portion of the projectile. The first signal observed corresponds to the expected arrival of the stress wave at the gage.

It appears that the applications of the mutual-inductance gage are not as restricted as we had formerly feared. In this experiment, a

separation of 51 mm was sufficient to isolate the gage from perturbations by a conductor moving at 0.77 km/s. It should be practical to develop shielding techniques to permit use of the mutual-inductance gage in an electrically noisy environment.

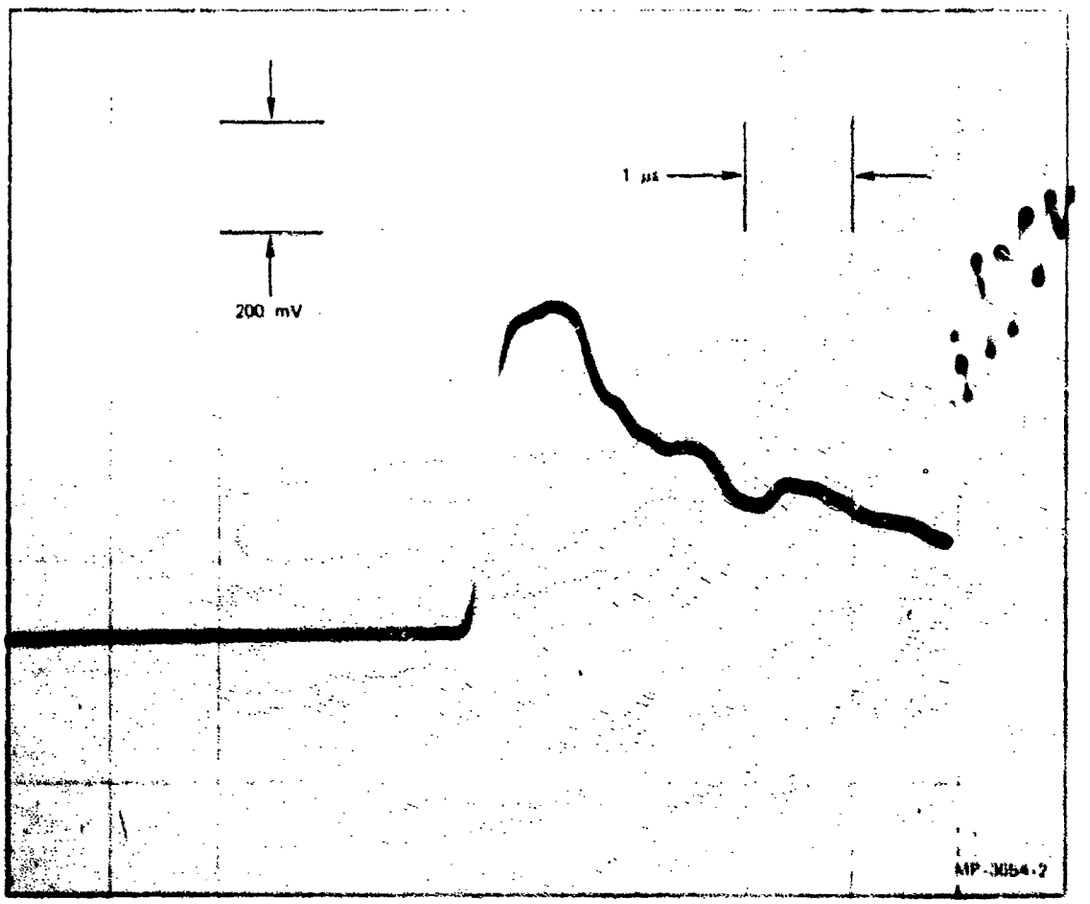

FIGURE 10 MUTUAL-INDUCTANCE GAGE RECORD, 0.6 km/s PEAK PARTICLE VELOCITY

IV HUSKY PUP DEBRIS COUPLING EXPERIMENT

The Husky Pup Debris Coupling Experiment (DCE) was motivated by the need to test the accuracy of computational modeling of the shock wave produced by the impact of debris accelerated by a nuclear explosion. In essence, the problem was to design a practical physical experiment that would also be simple and unambiguous, from a computational viewpoint. The experiment chosen was the impact of device-accelerated debris on a surface of a large block of homogeneous material. Transducers within the block would provide data on shock-wave parameters for comparison with computational results. The block had to be large, so that neither the transducers nor the computation would be affected, over the times of interest, by shock-wave interactions originating at lateral material interfaces.

The largest size block compatible with tunnel dimensions of the Husky Pup experiment would be a cylinder about 8-feet (2.4 m) in diameter; with this maximum diameter, a length of 10 feet (3 m) would be sufficient. Granite was chosen as the material for the block because it met all of the experimental requirements and was much less costly than alternative materials such as metals or glasses. To minimize fabrication costs, the cylindrical cross-section was approximated by an octagonal shape, 8 feet (2.4 m) across the flats.

The center of one end of the granite quasi-cylinder was to be impacted by the debris. Flat-bottomed holes, 4 inches (0.1 m) and 8 inches (0.2 m) diameter, were core-drilled from the other end of the quasi-cylinder with their axes directed toward the working point. Aluminum-shielded core assemblies, containing various in-granite shock-wave transducers were to be placed in these holes. An essential experimental requirement was that the shock propagation characteristics of the core assemblies match the surrounding granite as closely as possible.

SRI was initially committed to design, fabricate, test, and field six manganin stress gages in the Husky Pup DCE. We actually fielded six active manganin stress gages, one background (unpowered) manganin gage, and one aluminum temperature gage. Despite power supply failure, apparently the result of preshot flooding of the power supply alcove, excellent shock-wave time-of-arrival data were obtained that complement the time-of-arrival data obtained by the other DCE experimenters. These time-of-arrival data, together with available equation-of-state data on granite, indicate that actual stresses at various propagation distances were approximately double the computationally predicted values.

It must be noted that the DCE was an add-on to a previously planned and tightly scheduled nuclear experiment. Planning of the DCE took place concurrently with the laboratory development of the experimental techniques that were used; improvements in the design of the DCE were being made within 2 months of the scheduled Husky Pup execution date. In this section we initially discuss the laboratory studies that were performed in support of the design of the DCE. These studies were: measurement of granite resistivity at high shock stresses, in-granite manganin gage experiments, and EMP simulations to test shielding designs. We then discuss gage system design and construction, fielding, and experimental results of the DCE.

Laboratory Measurements

Granite Resistivity at High Shock Stresses

Two experiments were performed to measure the electrical resistivity of Raymond granite at high shock stresses. Granite samples 2 mm thick by 20 mm square were mounted on the copper base plates of Experiments 3654-1-3 and 3654-1-4. Each sample was backed by an anvil made up of a copper electrode 3.1 mm in diameter surrounded by a close fitting Lucalox ring 12 mm O.D. In order to avoid air-filled spaces, which would ionize

under shock loading, the assemblies were bonded with 0.01-mm-thick layers of Homalite 1100 epoxy. A 1-ohm viewing resistor was connected in parallel with the sample--i.e., between the base plate and the rear copper electrode. Prior to shock arrival at the sample, a constant-current pulse of about 5A was passed through the resistor, and the voltage across the resistor was monitored with an oscilloscope. A substantial decrease in the resistivity of the granite sample would produce a voltage decrease due to shunting of the 1-ohm resistor.

The experiments were designed to measure sample resistivities over the range of interest for gage design purposes, from about 0.02 ohm-cm to about 100 ohm-cm. For values outside that range, we obtain only upper or lower limits. One may note that if the sample resistivity at pressure exceeds 100 ohm-cm, the shunting of in-material manganin gages will be negligible, for any reasonable gage design. For sample resistivities below 0.02 ohm-cm, the gages will have to be insulated with some other material.

Excellent records were obtained in the two experiments, with copper-base-plate stresses of 150 GPa and 95 GPa. Because of the lower shock impedance of granite, relative to copper, the initial shock transmitted into the sample was less than half the base-plate stress, but the granite approached stress equilibrium with the base plate via successive shock reflections from the anvil and the base plate alternatively. It should be noted that the internal energy increase associated with a peak stress reached via reflected shocks will generally be lower than the internal energy associated with a peak stress reached via a single shock. Voltage decrease steps on both records could be time-correlated with the arrival of the first shock at the rear electrode and/or arrival of reflected shocks at either the base plate or the rear electrode. The resistance of the shunt path through the sample is calculated from the voltage ratio, and a raw resistivity

is calculated by assuming that the sample area is equal to the area of the rear electrode, and that the sample length is equal to the initial sample thickness. The raw resistivity can be corrected for the decrease in sample thickness due to shock compression and for the fringing-field effect. We can also estimate the magnitude of the correction that results from our use of epoxy to bond the assembly. Keeler has stated that epoxy becomes a good conductor above about 30 GPa; we interpret this to imply a resistivity below 1000 ohm-cm. We measured the resistivity of epoxy to be about 2 ohm-cm at 70 to 80 GPa in a reflected-shock experiment. In the granite resistivity experiments, the epoxy correction is negligible, provided that the epoxy resistivity is in the range of 1 to 100 ohm-cm at the pressures of interest. If the epoxy resistivity is as high 1000 ohm-cm at pressure (which we consider highly unlikely), it has the effect of a 10-ohm resistor in series with the granite, and our inferred granite resistivities err on the low side. If the epoxy resistivity is substantially lower than the granite resistivity at pressure, the area of the rear electrode is effectively increased, and our granite resistivities err on the low side. In Table 2 we include an estimate based on reasonable extremes of epoxy behavior.

In-Granite Gage Experiments

Experiments with in-granite manganin gages were initiated as soon as it became evident that granite would probably be used in the Husky Pup Debris Coupling Experiment. Initially we used Bradford granite, because it was on hand, but Raymond (Husky Pup) granite was used for the later experiments. The major purpose of these in-granite gage experiments was to provide us with information and experience applicable to the design of in-granite gages for the Debris Coupling Experiment. Accordingly, most of the in-granite gage experiments were add-ons to

Table 2

GRANITE RESISTIVITY MEASUREMENTS

Stress	Raw Resistivity	Resistivity after Thickness and Fringing Corrections	Resistivity and Additional Corrections for Extremes of Epoxy Behavior
39 GPa (1st shock)	> 40 ohm-cm	> 100 ohm-cm	> 100 ohm-cm
74 GPa (1st refl.)	3.5	10	5-15
88 GPa (2nd refl.)	1	3	2-6
67 GPa (1st shock)	4	12	6-18
120 GPa (1st refl.)	1	3	2-6
140 GPa (2nd refl.)	0.3	1	0.5-1.5

The results of these granite resistivity measurements indicated that it would be necessary to use carefully designed gages of very low impedance to minimize the shunting effect.

gage calibration experiments. In general, the uniform stress region of a base plate was reserved for time-of-arrival pins and calibration experiments; the less uniform (but higher peak-stress) region was used for the in-granite gage assemblies.

The first in-granite gage records were extremely noisy. Since the onset of the noise coincided with shock arrival at the granite, about 300 ns prior to shock arrival at the gage plane, we inferred the noise to be piezoelectric, ascribable to the compression of quartz crystals present in the granite. Our initial approach to the noise problem was to increase the gage viewing current, thereby increasing the signal and the signal-to-noise ratio. Subsequently, when it became apparent that transformer coupling would be necessary in Husky Pup (to make the transition between 100-ohm RG-22 and 50-ohm RG 331), we tested a commercial off-the-shelf transformer in an in-granite gage experiment. Despite an impedance mismatch (the transformer was designed for 75-ohm and 124-ohm cable) the transformer worked very well and also served to filter out most of the piezoelectric noise. Accordingly, custom transformers were ordered for Husky Pup use. Additional tests, including some dedicated experiments with long pulse duration explosive-in-contact geometries, were performed to test the longer-term survivability of various gage geometries and to test the performance of the prototype Husky Pup gage system under simulated field (long cables) conditions.

In the course of these in-granite gage experiments, we observed an apparent anomaly in gage response at stresses in granite above an estimated 60 GPa. Although the in-Vistal gage records on the same base plate were clearly flat-topped, in accordance with the stress wave shape expected from flyer-plate impact, the in-granite records indicated a triangular stress wave shape. These in-granite records could be interpreted as the result of shunting, the result of gage placement in

a nonunifrom stress region, or the result of stress relaxation caused by phase transformations in the granite.

In the final tests of in-granite gages, the uniform stress region of the base plate was used. Time-of-arrival pins (for stress calibration) and in-Vistal gages were also placed in the uniform stress region. Each granite assembly contained a Lagrangian array of three 0.05-ohm gages (identical in impedance with Husky Pup gages). The experiments also served as a test of the Husky Pup field power supplies and custom signal transformers. Two base-plate assemblies, each of which contained stress calibration pins, and one in-granite Lagrangian gage experiment, were shock-loaded by replicate flyer-plate systems. On the basis of the base-plate stress (determined from the pin records) and existing Hugoniot data for granite, one could predict flat-topped stress records, with the manganin resistance change corresponding to a peak stress of 65 GPa, and with no attenuation of peak stress over the wave propagation distance spanned by the gage planes.

In both experiments the gage records obtained differed substantially from these predictions. The stress waves were not flat-topped, the peak stress inferred from the manganin resistance change was 80 GPa, and peak stress attenuated sharply with distance of wave propagation into the granite. The in-Vistal records did show a flat-topped peak of the predicted duration.

We interpet these results in terms of the phase transition behavior of quartz and feldspar, major constituents of Raymond granite. The granite shocks up to a metastable state and begins to transform to denser phases, resulting in the observed stress relaxation. We infer that currently accepted Hugoniot data for granite (and perhaps for other rocks, as well) may be significantly in error in the stress region above about 50 GPa. The discrepancy between our results and earlier work is

ascribable to the rapid attenuation of the shock in granite, a phenomenon that was not easily measured before the development of in-material stress gages.

In terms of the internal energy increase of the shock-compressed material, we conservatively estimate 20% higher values than would be predicted from earlier Hugoniot data, assuming the same stress-wave input (corresponding to our experiments) for both estimates.

EMP Simulations

To minimize shunting by shock-induced conductivity of the granite, it was necessary to use manganin gages of very low impedance (0.05 ohm) in the Husky Pup experiment. Viewing current was to be limited to about 20 A to avoid excessive I^2R heating of the gages. Anticipated manganin resistance changes at pressure were of the order of 200%, and the corresponding signal would be about 2 V. Effective EMP shielding of the system was therefore critical.

A simple mockup of the gage system was constructed and tested in a simulated EMP environment. These tests were designed and performed by Art Whitson and Robert Bly of SRI's Electromagnetic Science Laboratory. Although the primary purpose of these tests was to discover and correct any weaknesses in the design of the gage system, the tests also provided excellent training for the personnel who would install the field system.

The EMP was simulated by a triggered capacitor discharge into a terminated transmission line, one leg of which consisted of the mockup of the proposed gage system. Crucial elements of the mockup (gage placement and layout, shield placement, cable types, signal transformer, and power supply) were identical with the field system. Granite was conservatively modeled by styrofoam, and cable lengths were necessarily much shorter than field lengths, but these differences did not affect the validity of the simulation. Capacitor voltages of up to 50 kV were

used to drive currents up to 600 A in the outer shield of the mockup, and voltages induced in the gage circuit were monitored through the output of the signal transformer.

These tests disclosed the need for additional shielding of the power and signal cables in the region between the granite block and the power supply. The added shielding of a double layer of copper braid surrounding the power-signal cable pair for each gage performed well in the simulation tests and was used in Husky Pup.

These tests also disclosed the vulnerability of the power supply enclosures to RF penetration via the ac line and via control and status indication cables. Robert Ely designed an appropriate system of filters, surge arrestors, an isolation transformer, and a power contactor to harden the ac line entry. Hardening of the control and status indication cables (or power supply redesign) did not appear possible within the available time before Husky Pup execution. The only apparent solution was to disconnect these cables during the period of last possible access to the power supply alcove. It would also be necessary to disable the power supply crowbar circuits at this time. No further tests of the gage system would be possible prior to the actual experiment, for without the crowbar circuit, which limits the length of the current pulse through the gage, the gages would be destroyed in dry runs. Furthermore, there would be no way of determining whether the power supplies were operative immediately prior to the execution of Husky Pup.

Gage System Design and Construction

The essential components of the system were four-terminal in-granite gages (seven manganin piezoresistive stress gages and one aluminum-resistance temperature gage), down-hole power supplies, recording instruments, cables, and shielding. It was necessary to use very-low-impedance manganin gages in order to minimize shunting due to shock-induced

(and perhaps also radiation-induced) electrical conductivity of the granite. Four-terminal measurements were necessary, as opposed to two-terminal measurements, in order to accurately measure the resistance changes of the low-impedance gages. Because of the limited number of up-hole cables available, it was necessary to put the power supplies in an alcove near the Working Point, thereby reducing the number of required high-quality up-hole cables from 32 to 8.

The severe EMP environment necessitated exceptionally good shielding, combined with the highest possible signal levels. In a four-terminal resistance measurement, the voltage output is IR, the product of the gage resistance and the viewing current, but the heating effect of the current is proportional to I^2R. Since the manganin gage would be subjected to a large temperature increase on shock compression and a temperature increase due to radiation, we arbitrarily decided to limit the additional I^2R heating to the amount that would produce a $100^{\circ}C$ rise over 200 μs. This limit corresponded to a viewing current of about 20 A, and the expected resistance-increase signal at 100 GPa (one megabar) would be about 2 V, for a manganin gage having an initial resistance of about 0.05 ohm.

The basic requirement for the power supply was that it supply a constant current of 20 A for a period of about 200 μs. The power supply must be triggerable, so that the current pulse can be started at a predetermined time before arrival of the stress wave at the gage. To permit test pulsing of the gage, one needs a "crowbar" circuit to shut off the current pulse before the gage is destroyed by excessive heating. In the actual experiment, however, the crowbar is unnecessary and is preferably disconnected, to ensure that the current pulse is not shut off prior to stress-wave arrival at the gage.

A simple capacitor-discharge system, essentially a modified version of the standard manganin gage power supply developed at SRI 12 years ago, was designed to meet the power supply requirements. A simplified diagram of the gage system is given in Figure 11. The power supply is basically a charged capacitor in series with a switch (SCR) and various resistances, including the gage resistance. The capacitor has a value of 1000 μF and is charged to 500 V; the sum of the series resistances is about 25 ohms. With an RC time constant of 2.5×10^{-2} s, the initial 20-A gage current decays by only 1% over a period of 250 μs, assuming that the series resistance remains constant. The series resistance is composed of a 20-ohm ballast resistance, a 3.4-ohm cable resistance (over the run between the power supply and the granite block), the 0.05-ohm gage resistance, and about 0.2 ohm for the resistance of the gage leads in the granite block (from the gage plane to the rear of the granite block). We can neglect the shunting effect of the signal circuit resistance (> 100 ohm) in parallel with the gage resistance.

Upon stress-wave arrival the resistance of the gage element will increase by about 220% for 100 GPa (one megabar). The manganin portion of the current leads (about 0.05 ohm in the gage plane) will increase in resistance similarly. The manganin leads are welded to copper foil leads that will be progressively shock-heated as the shock propagates through the granite. As a result of the shock heating, the copper leads will increase in resistance by 300 to 400%. Since we wanted to continue recording manganin resistance over about 10 μs after shock arrival, the change in resistance of the copper leads in the region near the gage had to be considered. We minimized the effect by keeping the copper foil lead resistance low (about 0.02 ohm) over the region between the gage plane and a transition plane about 10 cm downstream, where the foil leads were joined to #16 copper wire leads, which ran to the rear of the granite block. Although gage failure was expected

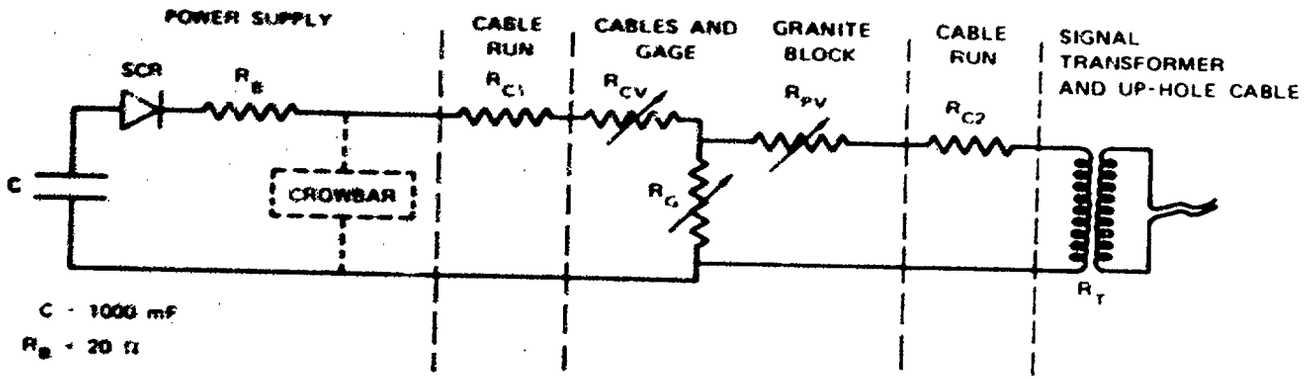

FIGURE 11 SIMPLIFIED DIAGRAM OF HUSKY PUP MANGANIN GAGE SYSTEM

to occur before the shock reached the transition region, we must note that the #16 copper wire leads (about 0.08 ohm initial resistance) would be subject to radiation preheat and could possibly double in resistance over the period of time between nuclear zero and shock wave arrival.

The total of these resistance changes is small--less than 2% of the initial series resistance of the discharge circuit--and the constant-current conditions are not substantially changed.

The full power supply schematic diagram is given in Figure 12. Since 1000-μF capacitors of the required voltage rating were either not available in time or were prohibitively expensive, series-connected 2000-μF capacitors were substituted. The circuit was laid out symmetrically, to minimize EMP problems. As noted previously, the ready-light circuit and the crowbar circuit were disconnected prior to the actual experiment. The peak capacitor voltage is regulated by a zener string; isolation resistors between the zener string and the capacitors provide protection against the effects of radiation-induced zener failure at nuclear zero (perhaps a remote possibility). The temperature-gage power supply differed only in its use of 50-ohm ballast resistors, limiting viewing current to 5 A.

A complete power supply, including the capacitor charging circuit, was constructed for each active gage. Mil-spec (125C) components were used, in recognition of possible high temperatures in the instrumentation alcove during grout curing, and the circuits were potted in silicone rubber for moisture protection. The power supplies were thoroughly bench-tested and they were also use-tested in laboratory experiments on the dynamic response of in-granite gages. The field power supply container was a compartmented steel box, 1.6 m long by 0.4 m wide by 0.23 m deep. The box was welded from 3.2-mm-thick steel; the removable top cover plate, also 3.2-mm-thick steel, was secured by 10-24 machine

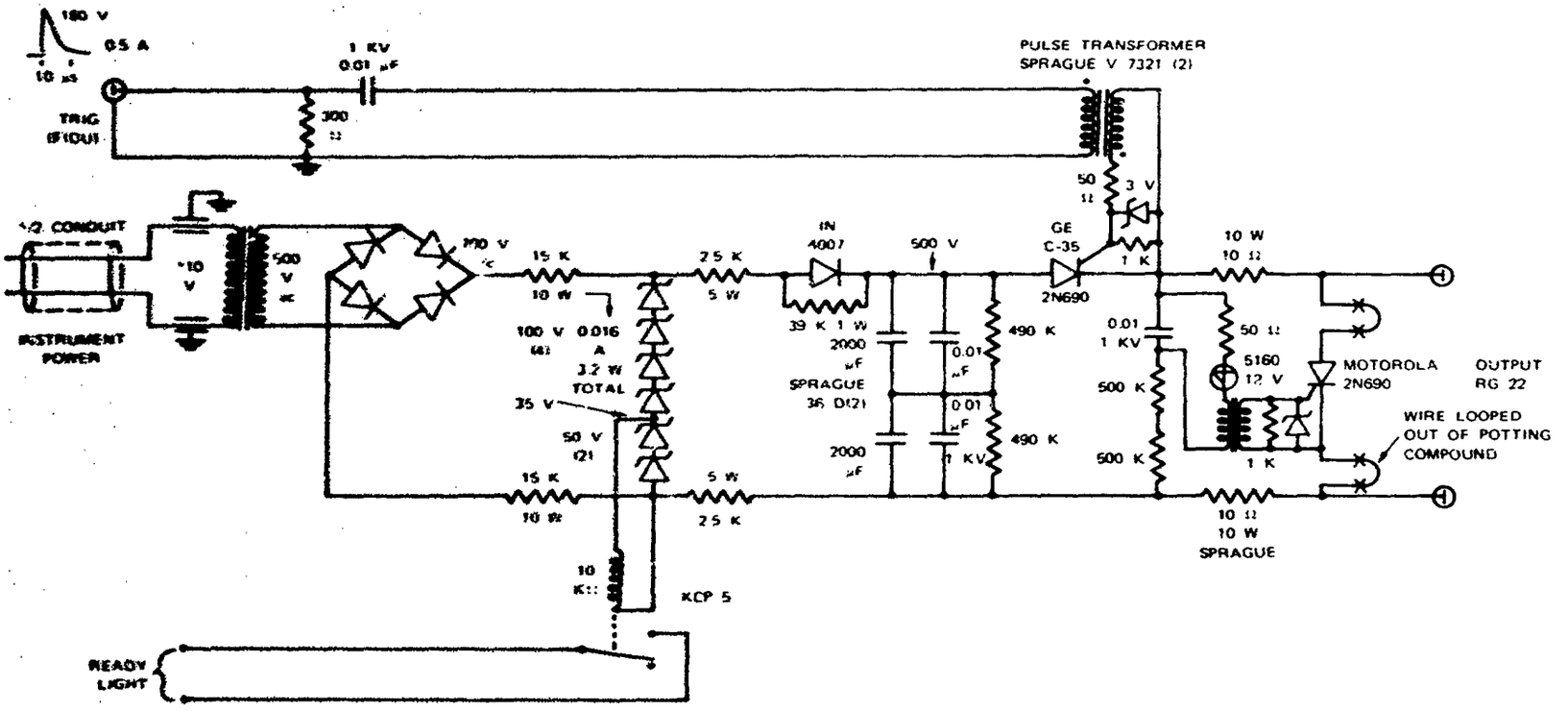

NOTE T1N0 SCR must be GE C 35 2N690 for reliable TRIG and hold off current spec

MA-3654-32

FIGURE 12 HUSKY PUP POWER SUPPLY SCHEMATIC

screws spaced 20 mm apart. Within the box, compartment covers of 1.6-mm-thick steel served to individually shield each power supply. All welds were continuous and hole-free; closures were designed with wide mating areas to permit bonding with conductive epoxy (in addition to the machine screws) at final button-up. The final test of the power supplies prior to fielding was a 60-hour burn-in (ac power on) in the closed field container, to ensure that no overheating problems would develop in the field.

The topology of the shielding is illustrated in Figure 13. The granite core assemblies were shielded by closely fitting containers welded from 3.2-mm-thick aluminum. These containers were connected through a steel bellows to a large compartmented steel J-box at the rear of the granite block. Each gage assembly within a core was individually shielded by two layers of aluminum with a total thickness of 0.3 mm. The aluminum shielding was bonded to 1-mm-wall thickness copper pipe that provided additional shielding for each pair of RG22 cables over the run from the rear of the granite core into the J-box. Over the run between the J-box and the power supply alcove, there were two continuous layers and one partial layer of shielding. The continuous layers consisted of a double copper braid spun over a pair of RG-22 cables and soldered to nipples at both the J-box and power supply ends, and the outer shield (double copper braid) of each RG-22 soldered to nipples on inner partition walls of both the J-box and power supply box. A partial shield was provided by steel conduit welded to the J-box and terminating in an open end at the bypass-bypass extension intersection. The up-hole cable shields provided continuity between the power supply box and the instrumentation trailer. It must be emphasized that the topology of the shielding was not violated in actual practice. All shields were hole-free, and all shield connections were made by welding, soldering, or large-area conductive epoxy bonds. The ac line-hardening measures are also illustrated in Figure 13.

The granite core assemblies are illustrated in Figures 14 and 15. These assemblies were built up of closely fitting individual granite pieces, bonded by Al_2O_3-loaded epoxy. Note that the gage and the foil leads lie in a plane parallel to the direction of shock propagation; this edge-on geometry gave long gage survival times in laboratory experiments. The leads remain parallel to the shock direction and widely spaced for about 10 cm downstream of the gage element, at which point the lead spacing is narrowed, the leads jog, and connections are made to #16 copper wire. The copper wire was epoxied into grooves cut in pieces of granite. For the closest-in gages, the cross-sectional area of the shielded region was reduced from 15.3 cm^2 at the gage to 4.6 cm^2 at the transition to #16 wire. This reduction in shield area was made to reduce EMP vulnerability. The shield area had to be larger in the vicinity of the gage in order to reduce shunting through shock-compressed (electrically conductive) granite.

The preheat temperature gage was a grid photoetched from ordinary household aluminum foil, 0.025 mm thick, and had an initial resistance of 0.463 ohm. This is simply a four-terminal resistance thermometer; the change in resistance is proportional to the preheat temperature, and the recording scheme is identical with that used for manganin stress gages. Aluminum was used because it has nearly the same atomic number as the surrounding granite and should therefore be heated similarly by radiation. The use of aluminum, as opposed to nickel or platinum (conventional resistance-thermometer materials), permits one to avoid the problem of heat transfer between the gage and the granite. We would have preferred to use a gage of much higher resistance, since the temperature gage was intended to record only prior to stress-wave arrival and shunting was not a constraint. We did try to make a higher-impedance gage, but we could spend only one day at it (without compromising the fielding schedule), and we had to accept the lower-impedance gage.

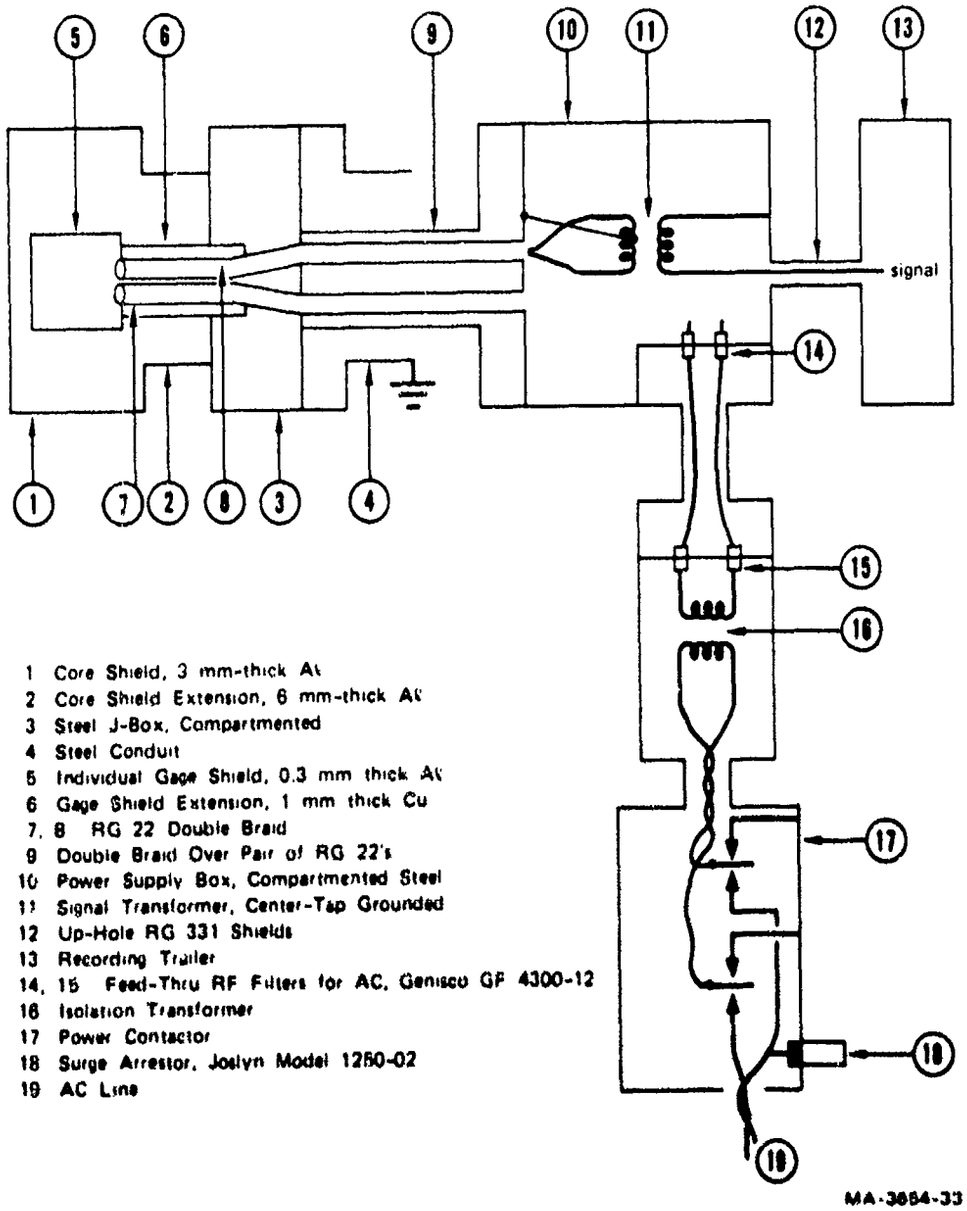

1 Core Shield, 3 mm-thick Al
2 Core Shield Extension, 6 mm-thick Al
3 Steel J-Box, Compartmented
4 Steel Conduit
5 Individual Gage Shield, 0.3 mm thick Al
6 Gage Shield Extension, 1 mm thick Cu
7, 8 RG 22 Double Braid
9 Double Braid Over Pair of RG 22's
10 Power Supply Box, Compartmented Steel
11 Signal Transformer, Center-Tap Grounded
12 Up-Hole RG 331 Shields
13 Recording Trailer
14, 15 Feed-Thru RF Filters for AC, Genisco GF 4300-12
16 Isolation Transformer
17 Power Contactor
18 Surge Arrestor, Joslyn Model 1250-02
19 AC Line

FIGURE 13 HUSKY PUP SHIELDING TOPOLOGY

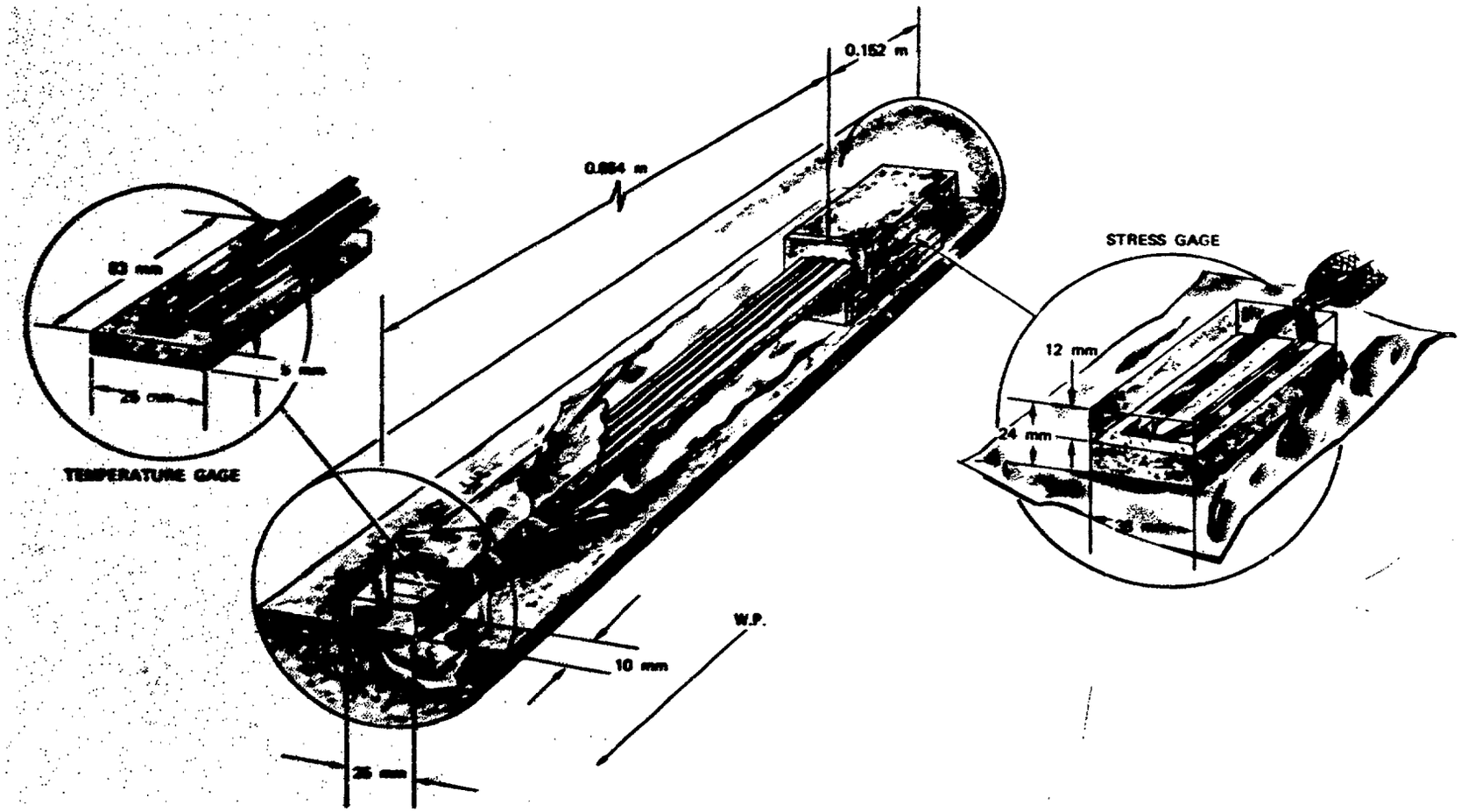

FIGURE 14 4-INCH DIAMETER (101.6 mm) GRANITE CORE

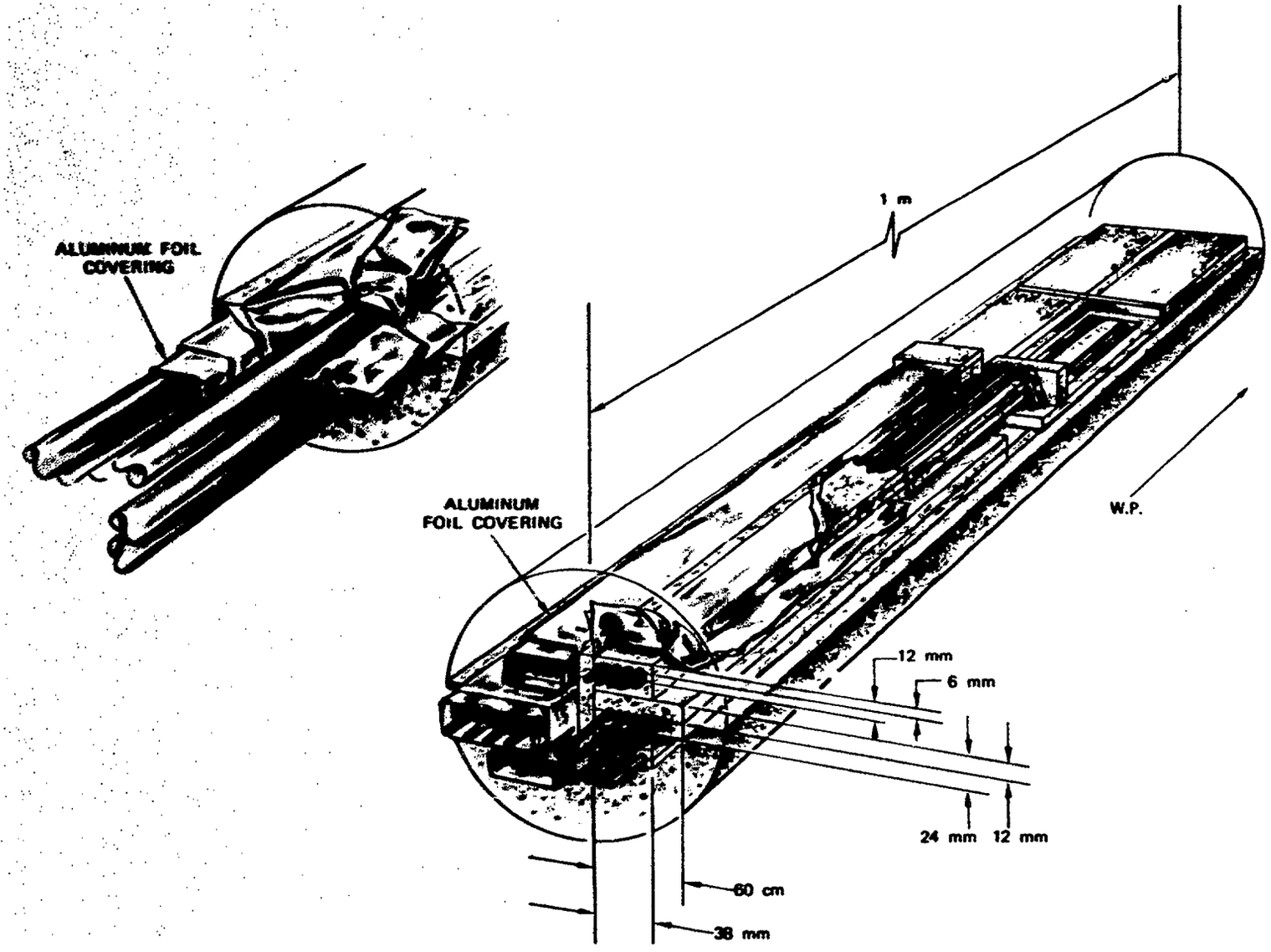

FIGURE 15 8-INCH DIAMETER (203.2 mm) GRANITE CORE

MP-3654-35

On the basis of preshot calculations, the temperature gage was placed at a distance corresponding to about 250 GPa. Two manganin gages, one of which was an unpowered background gage, were placed at the predicted 100-GPa range. Two more gages, with high impedances of 0.305 ohm and 0.05 ohm, respectively, were placed at the predicted 80-GPa range. The purpose of the different impedances was to provide data on the magnitude of the shunting effect. One gage was placed at each of the ranges corresponding to stresses of 60 GPa, 40 GPa, and about 35 GPa.

Fielding

The granite cores were installed on schedule, and the entire gage system, from the granite block to the recording trailer, was completed in time for about a week of dry runs prior to MFP. No problems with the system were encountered in any of these dry runs, including MFP. After MFP, we disconnected the crowbar circuits and status indication cables, and the alcove was sealed off by a grout pour.

Unfortunately, the grout pour fouled the alcove dewatering system and the alcove completely flooded. The water rose well above the top of our power supplies and the water pressure was estimated to have been about 10 atmospheres (1 MPa). The alcove was subsequently reentered. The power supply box was full of water, and the ac contactor was badly corroded. After the water was emptied out of the power supply box and the power supplies were dried off, the power supplies were tested, and found in perfect working order. The potting had prevented any damage. After replacement of the ac contactor, the entire gage system was checked out under partial power. Since the crowbars were disconnected, we allowed the capacitors to charge up to only 50 V (instead of the normal 500 V) before discharging them through the gages. This was a more severe test of the triggering system than a full power discharge. The power supply box was buttoned up again, and the alcove was sealed off, after installation of a new dewatering system.

Prior to Husky Pup execution, the alcove flooded again. The evidence relating to the water depth in this second flooding is contradictory. If one believes the water level gages, the depth did not exceed 3 feet. If one believes the manganin gage power supply status-indication lights (the terminals in the alcove were disconnected from the power supply but still "live"), the maximum water depth exceeded 4 feet.

Results

The recording instrumentation functioned perfectly, but the gage power supplies did not trigger. However, we obtained excellent time-of-arrival data from the piezoelectric signals produced by shock compression of the quartz crystals in the granite. One of the noise records is shown in Figure 16. For comparison, we show a record of a laboratory experiment with an in-granite gage Figure 17. This experiment was a test of the Husky Pup gage system: a Husky Pup power supply, custom signal transformer, a 0.05-ohm gage nearly identical to a Husky Pup gage, and granite cut from the Husky Pup Raymond granite block. The noise in this laboratory experiment began at the time of shock arrival at the granite, about 300 ns before shock arrival at the gage. Since the gages in Husky Pup were individually shielded, the first piezoelectric noise should appear after the shock wave enters the shielded region. In our experience with in-granite gages in laboratory experiments, the noise pickup invariably begins before the shock wave reaches the gage plane. In Husky Pup, the manganin gages were located ~ 1.5 cm behind the shield. In essence, there is a 1.5-cm uncertainty in the position of the shock front at the time of the first appearance of piezoelectric noise in our Husky Pup records. The time-of-arrival (TOA) data are listed in Table 3.

These data complement the TOA data obtained by the other granite block experimenters and confirm that peak stresses at various propagation

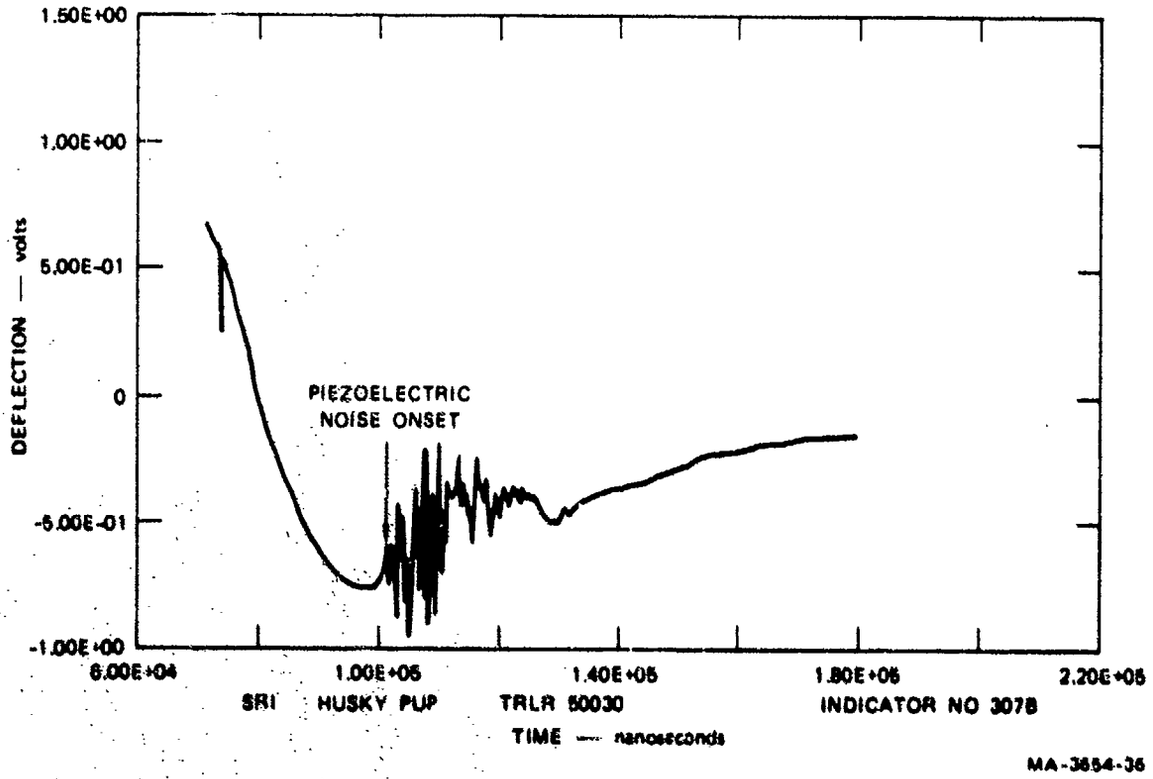

FIGURE 16 HUSKY PUP TIME-OF-ARRIVAL SIGNAL

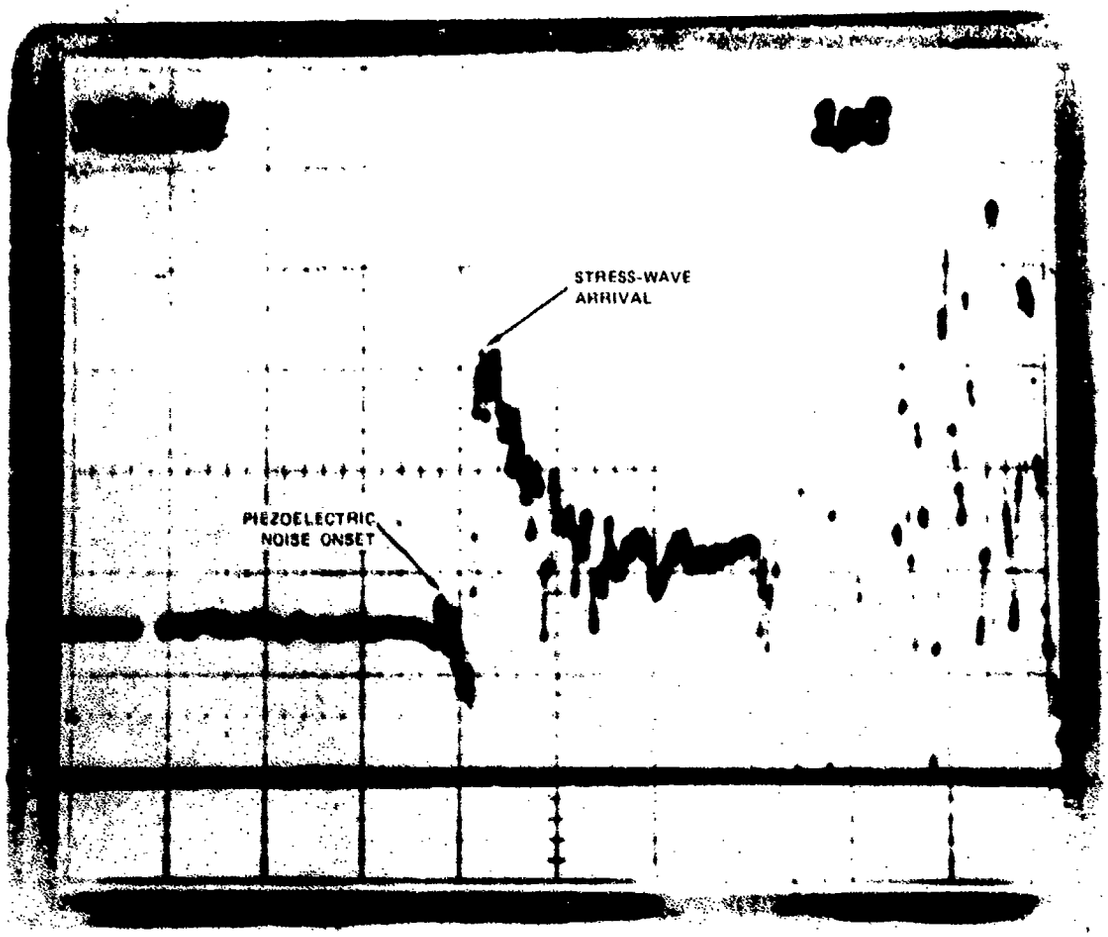

FIGURE 17 LABORATORY IN-GRANITE GAGE RECORD

Table 3

GRANITE BLOCK TIME-OF-ARRIVAL DATA

Channel	Core	Distance from Front of Granite Block, Measured in Direction of Core Axis (cm)		Time of Arrival After Nuclear Zero (μs)
		Shield Position	Gage Position	
308	0.1 m (temp. gage)	98.6	98.9	< 27.0
301	0.2 m	134	135.4	53.9
302	0.2 m	134	135.4	53.4
303	0.2 m	145.4	146.9	62.7
304	0.2 m	145.4	146.9	63.0
305	0.2 m	159.4	160.9	75.7
306	0.2 m	180.4	181.9	94.7
307	0.1 m	184.0	185.4	98.4

distances were about twice as high as pre-experiment predictions. Because of this gross error in prediction, only one of the manganin gages (the predicted 35 GPa) was actually located in the stress region below 100 GPa, the maximum stress at which we expect in-granite manganin gages to work. If the power supplies had triggered, the remaining gage records would probably have yielded only time-of-arrival information, albeit without the 1.5-cm uncertainty of the present data.

The EMP shielding measures were effective. In the manganin gage records, EMP noise levels had decayed to less than one volt in six of the seven cases (the seventh had a 2 V level) by the time of shock arrival at the gage (ranging from 50 to 100 us after nuclear zero).

The EMP noise was quasi-sinusoidal, with a period of about 10 us. The expected stress signals, based on preexperiment calculations, would be essentially triangular, rising within 1 us to a peak of about 2 V and decaying toward initial levels over about 10 us. Because of these essential differences between the noise and the expected signals, the signals would have been clearly discernible. If the power supplies had triggered and if the stress levels had been in the predicted range, the observed EMP noise would not have seriously degraded the accuracy of peak stress measurement.

In the temperature gage record, the noise levels are comparable with the expected signal level. Because of the character of the expected signal (a gradual rise from 2.5 V to about 7 V over 30 us), it is doubtful that good temperature data would have been obtained even if the power supplies had triggered.

Discussion

It is not possible to determine why the power supplies failed to trigger. The same signals successfully triggered oscilloscopes in the recording van. The trigger cable connectors in the alcove may have

been short-circuited by water several days before the shot when the alcove flooded. More likely, however, the ac power to the power supplies was lost, possibly by corrosion of the ac contactor points.

It must be recognized that measurements of stress-wave propagation at very high stresses (100 GPa and above) are difficult and entail a high risk of failure, even without the problems (large induced electric fields, neutron, gamma, and X-ray fluences) associated with the nuclear test environment. The results of the Debris Coupling Experiment clearly demonstrate the feasibility of close-in measurements; the major environmental problems were successfully surmounted. The manganin gage appears to be a useful close-in stress transducer, and, given advance warning, it would be simple to build a submersible power supply. Preheat temperature measurements also appear feasible; the necessary higher signal levels could be easily obtained, given sufficient lead time to construct a high-impedance resistance thermometer.

The detailed plan of the DCE evolved during a series of planning meetings chaired by Dr. C. P. Knowles of RDA and attended by experimenters and theoreticians from various agencies including LASL, LLL, SAI, EG&G, PI, AFWL, SSS, IRT, SLA, SRI, and DNA. The extraordinary feature of these meetings was the prevailing spirit of working toward a common goal. There was free exchange of ideas and criticism, all directed toward a successful solution to the experimental problems. Design decisions were deferred until the last possible moment, in order to take advantage of information gained from concurrent laboratory experiments. The schedule was so tight that there was little time for the DCE experimenters to participate in Husky Pup dry runs, but it would appear that the additional time spent in planning and in laboratory experiments adequately compensated for the missed dry runs and made possible a state-of-the-art nuclear experiment.

REFERENCES

1. T. J. Ahrens and J. T. Rosenberg, "Shock Metamorphism: Experiments on Quartz and Plagioclase," in Shock Metamorphism of Natural Materials, B. M. French and N. M. Short, eds. (Mono Book Corp., Baltimore, Md. (1968).
2. D. E. Grady, W. J. Murri, and P. S. De Carli, J. Geophys. Res., 80, 4857-61 (1975).
3. D. E. Grady, W. J. Murri, and K. D. Mahrer, J. Geophys. Res. 81, 889-93 (1976).
4. P. W. Bridgman, Proc. Am. Acad. Arts Sci. 47, 321 (1911).
5. E. Lisell, Diss. Upsala (1902), Referenced by Bridgman in Physics of High Pressure (G. Bell, London, 1958).
6. P. J. A. Fuller and J. H. Price, Nature 193, 262-3 (1962).
7. D. Bernstein and D. D. Keough, J. Appl. Phys., 35, 1471-4 (1964).
8. R. N. Keeler and E. B. Royce, "Shock Waves in Condensed Media" in Physics of High Energy Density, XLVIII Corso (Academic Press, New York, (1971).
9. E. Barsis, E. Williams, and C. Skoog, J. Appl. Phys., 41, 5155-62 (1970).
10. L. M. Lee, J. Appl. Phys. 44, 4017-22 (1973).
11. J. H. Price, private communication to P. S. De Carli (1968).
12. D. D. Keough, "Procedure for Fabrication and Operation of Manganin Shock Pressure Gages," Technical Report AFWL-TR-68-57, Air Force Weapons Laboratory (August 1968).
13. D. D. Keough and J. Y. Wong, J. Appl. Phys. 41, 3508-15 (1970).
14. A. N. Dremin and G. I. Kanel, Fizika Goreniya i Vzryva 8, 147-9 (1972).
15. J. W. Lyle, R. L. Schreiver, and A. R. Mc Millan, J. Appl. Phys. 46, 4663-4 (1969.
16. J. T. Rosenberg, M. J. Ginsberg, and R. F. Williams, Bull. Am. Phys. Soc., Series II, 17, 1099 (1972).

Appendix

SUMMARY OF SHOCK-LOADING EXPERIMENTS

Flyer-Plate Experiments

In all of these experiments, flat-topped stress waves were produced by the impact of an explosively accelerated metal flyer plate on a metal base plate, on which gage packages were mounted. Coaxial shorting pins were used to measure flyer-plate velocity, shock velocity in the base plate, free surface velocity of the base plate, and planarity of flyer-plate impact. In every case, the explosive was an 203 mm (8 inch) diameter pad of PBX (plastic bonded HMS), initiated by an 203 mm (8 inch) diameter plane-wave lens. There was a 1.5 mm (1/16 inch) air gap between the PBX and the metal flyer (to minimize flyer-plate spall), and the flyer plate was accelerated over a free run of 28 mm (1.1 inches) of air. The experimental variables were PBX thickness, flyer-plate thickness, flyer-plate material, base-plate thickness, base-plate material, and the gages themselves (method of construction, insulator material, etc.).

3654-1-1 102 mm-thick PBX, 4.76 mm thick type 304 stainless steel flyer, five manganin gage packages on the base plate. Two gages were packaged in Vistal (fully dense Al_2O_3 ceramic), two gages were packaged in fused silica, and one gage was packaged in granite. One each of the Vistal and silica packages was bonded by Cabal glass (2-1-9 molar ratios of CaO, Al_2O_3, and B_2O_3, respectively). The other gage packages were bonded by Al_2O_3-filled epoxy (equal weights of Al_2O_3 powder and Homalite 1100 epoxy), with relatively thick (0.25 mm) bond lines. Initial gage resistances were ~ 0.2 ohm.

Results: Both Cabal-bonded gages failed about 50 ns after shock-wave arrival. The other gages worked reasonably well, surviving through partial stress release (~ 150 ns for Vistal, ~ 800 ns for silica and granite packages). Pin records were not obtained because of oscilloscope malfunction; stress in base plate is estimated (based on explosive-to-flyer-plate mass ratio and previous experience) at about 130 GPa (1.3 Mbar). Corresponding stresses in gage packages are ~ 45 GPa in silica, ~ 57 GPa in granite, and ~ 107 GPa in Vistal. On the basis of subsequently determined manganin calibration data, observed resistance changes are concordant with estimated stresses, but Vistal gage response is obviously degraded by excessive bond thickness.

3654-1-2 76 mm thick PBX, 4.65 mm thick 304 S.S. flyer, 4.27 mm thick OFHC copper base plate, and five gage packages. Gage packages were Vistal (two gages), fused silica (two gages) and granite. One vistal package was Cabal-bonded, remaining gages were bonded with Al_2O_3-loaded epoxy (~ 0.25 mm bond lines). Initial gage resistances were about 0.2 ohm.

Results: The Cabal-bonded gage failed about 100 ns after shock arrival; the other gages survived through partial stress release. Pin records were not obtained; estimated stress in copper is about 100 GPa (1 Mbar), based on explosive-to-flyer-plate-mass ratio; the in-silica manganin gages indicate a stress of about 36 GPa, implying a stress in copper of 105 GPa and a stress in Vistal of about 88 GPa. Resistance changes in all gages are concordant with subsequent calibration results; the Vistal record was degraded by excessive bond thickness.

3654-1-3 127 mm thick PBX, 3.05 mm thick 304 S.S. flyer, 4.66 mm thick OFHC copper base plate, four gage packages, and two resistivity experiments. Gage packages were granite (two gages), Vistal, and fused silica, all bonded by Al_2O_3-loaded epoxy. One of the granite gages had a thick (0.33 mm) bond at the gage plane; the other gages had thin bonds (0.033 mm) including the 0.025 mm gage thickness. Reduction in bond thickness required modification of Al_2O_3-loaded epoxy (31 wgt% 0.3 micron Al_2O_3 powder, 69 wt% 1100 Homalite epoxy). Gage design was modified for lower initial resistance of about 0.15 ohm. Resistivity samples were Raymond granite and single-crystal MgO, backed by copper anvil-electrodes.

Results: The in-silica gage failed on shock arrival, remaining gages survived through partial stress release, good resistivity records were obtained, and pin records yielded independent measurement of stress in the copper base plate of 150 ± 10 GPa. Corresponding stress in Vistal was 122 ± 7 GPa, and observed peak resistance change, $\Delta R/R_o$ = 2.05, decayed about 10% over 400 ns. In retrospect, minor shunting appears to have occurred. The records from both in-granite gages were very noisy (due to piezoelectric noise), but observed resistance changes appeared lower than expected.

3654-1-4 102 mm thick PBX, 5.51 mm thick 304 S.S. flyer, 4.67 mm thick OFHC copper base plate, five gage packages, and one granite resistivity experiment. Gage packages were Vistal (two gages), fused silica (two gages), and granite, all with thin bonds. One of the Vistal packages was backed by aluminum, to provide a step release point, and one of the

silica packages was backed by PMMA (plexiglas) for step release. Initial gage resistances were ~ 0.15 ohm.

Results: One in-silica gage failed on shock arrival, two gages (one in-Vistal and one in-silica survived through stress release, and two gages (in-Vistal and in-granite) survived at least through partial stress release (the oscilloscope windows did not cover the full release). A good resistivity measurement was obtained, and excellent pin records were obtained. Based on the pin records, the stress in the copper base plate was 96 ± 2 GPa, and the corresponding stress in Vistal was 80 ± 2 GPa. The shapes of the in-Vistal records agree in detail with calculated stress-wave profiles. The in-silica record (32 GPa) and the in-granite record (40 GPa) are somewhat noisy but follow expected profiles and show resistance changes compatible with accepted manganin calibration data. The release steps (Vistal-aluminum and silica-PMMA) yield resistance changes that coincide with resistance changes on loading, and resistance hysteresis on release to zero stress is no more than about 5%.

3654-1-5 152 mm PBX, 3.05 mm thick tool-steel flyer, 4.83 mm thick OFHC copper base plate, and four gage packages. Gage packages were Vistal backed by aluminum (for step release), copper (the gage element was insulated from the copper by 0.1 mm-thick pieces of fused silica), aluminum-foil-shielded granite (the gage element was insulated from the foil by 0.15 mm thick layers of Al_2O_3-loaded epoxy), and unshielded granite. The Vistal and unshielded granite packages had thin (0.033 mm)

bonds in the gage planes. The unshielded in-granite gage was powered by a prototype 20-A constant-current supply and the signal was transformer-coupled (a test of the system proposed for use on Husky Pup). The in-granite gages had initial resistances of ~ 0.5 ohm; the in-Vistal and in-copper gages had initial resistances of ~ 0.15 ohm.

Results: The in-copper gage shorted on shock arrival and the shielded in-granite gage shorted about 20 ns after shock arrival. The in-Vistal gage and the unshielded granite gage survived through partial stress release. Excellent pin records yielded a stress in copper of 155 + 5 GPa, corresponding to a stress in Vistal of 125 + 5 GPa. The prototype Husky Pup system worked well.

3654-1-6 127 mm-thick PBX, 3.05 mm thick 304 S.S. flyer, 4.52 mm thick OFHC copper base plate, four gage packages. The gage packages (thin loaded epoxy bond) were Vistal backed by aluminum (two gages) and granite (two gages). One of the in-granite gages was aligned with its thickness (and the bond plane) normal to the shock front; the other in-granite gage was in the conventional parallel geometry. In-Vistal gage elements were initially ~ 0.15 ohm; in-granite gage elements were initially ~ 0.5 ohm.

Results: The parallel-geometry in-granite gage failed during stress rise; the other gages survived through partial stress release. Good pin records yielded a stress in the copper base plate of 150 + 10 GPa, corresponding to a stress in Vistal of 120 + 7 GPa. Observed gage resistance profiles agreed well with calculated stress-wave profiles.

3654-1-7 102 mm-thick PBX, 3.85 mm thick tool-steel flyer, 4.67 mm thick OFHC copper base plate, four gage packages. Gage packages (thin loaded epoxy bonds) were silica-insulated aluminum, silica-insulated copper, Vistal, and granite. The in-granite gage had an initial resistance of 0.5 ohm, the other gages were initially 0.15 ohm.

Results: The in-copper and in-aluminum gages shorted on shock arrival, the in-Vistal gage survived for about 100 ns at stress, and the in-granite gage survived through stress release. The pin records could not be deciphered, and the in-granite record was too noisy to be useful. The double-humped appearance and early failure of the in-Vistal record and the "noise" in the in-granite record can be interpreted as evidence of multiple shocks resulting from in-flight fragmentation of the flyer plate.

3654-1-8 127 mm-thick PBX, 5.33 mm-thick 404 S.S. flyer, 4.74 mm-thick OFHC copper base plate, four gage packages. Gage packages (thin loaded epoxy bond) were Vistal (backed by aluminum), silica-insulated aluminum, and granite. The fourth gage was in Lucalox (fully dense Al_2O_3 ceramic) bonded by ceramic strain-gage cement. The in-granite gage was initially 0.5 ohm, the in-Lucalox gage was initially 0.2 ohm, and the in-Vistal and in-aluminum gages were initially 0.15 ohm.

Results: All gages survived through partial stress release; good pin records yielded stress in copper of 105 ± 5 GPa. Corresponding stresses in Vistal (and Lucalox) and in aluminum were 88 ± 5 GPa and 57 ± 5 GPa, respectively.

The Vistal record was flat-topped and gave a step release point as planned. The ceramic cement-bonded Lucalox record showed a sharp rise to a resistance ratio in agreement with the Vistal record. However, the resistance rose by an additional 25% over the next 100 ns and then remained relatively constant until stress release. This additional rise is attributed to dimpling of the gage caused by interaction of the gage with the porous ceramic cement. The silica-insulated in-aluminum gage had a poor rise time (about 200 ns) and reached only about half the expected resistance change at stress. Shunting probably occurred.

3654-1-11 102 mm-thick PBX, 3.05 mm-thick 304 S.S. flyer, 4.95 mm thick 2024T6 aluminum base plate, two in-Vistal gages, and a three-gage in-granite Lagrangian array. One of the in-Vistal gages was backed by aluminum and used a 0.15-ohm element. The other in-Vistal gage used a 0.05-ohm element. The in-granite gages used 0.05-ohm elements powered by Husky Pup power supplies, and the signals were transformer-coupled.

Results: All gages survived through at least partial stress release, and the Husky Pup systems (0.05-ohm gages, 20-A power supplies, wideband signal transformers) worked very well. However, the records were somewhat noisy, and only the free-surface-velocity pin records were obtained. The in-granite gages indicated possible stress relaxation in granite. The 0.05-ohm in-Vistal gage showed an abnormally low resistance change at pressure; this effect is ascribed to a poorly positioned potential lead connection.

3654-1-12 102 mm-thick PBX, 3.05 mm-thick 304 S.S. flyer, 4.95 mm thick 2024T6 aluminum base plate, two in-Vistal gages, and a three-gage in-granite Lagrangian array. This shot was a repeat of 3654-1-11, with the addition of aluminum-foil shielding around the in-Vistal gages and around the in-granite array.

Results: All gages survived through at least partial stress release, the Husky Pup systems worked well, and excellent pin records were obtained. The additional shielding resulted in substantial noise reduction, and the possible stress relaxation in granite was again observed. The resistance change at peak stress was about 10% higher for the 0.05-ohm in-Vistal gage than for the 0.15-ohm in-Vistal gage. This result is interpreted as evidence of minor shunting.

Explosive-in-Contact Experiments

In these two experiments, relatively-long-duration (but attenuating) stress waves were produced by plane-wave initiation of a pad of explosive in contact with a metal base plate on which gage packages were mounted. The stress in the base plate was not measured independently of the gage measurements; these experiments were intended as test of the Husky Pup gage configuration and recording system over longer times than could be obtained with flyer-plate systems.

3654-1-9 P-60 152 mm-diameter plane-wave lens, 51 mm-thick PBX, 6.35 mm-thick 2024 T6 aluminum base plate, one active in-granite gage in parallel geometry. The Husky Pup power supply and signal transformer was used and the signal was transmitted over 400 meters of RG-8 cable, in simulation of NTS recording conditions.

Results: A good record was obtained; the gage survived for 4 μs before excessive lead stretch occurred.

3654-1-10 Repeat of 3654-1-9, except that the gage was in the edge on geometry.

Results: A good record; the gage survived for 8 μs before lead stretch became excessive.

Gas Gun Experiments

These experiments were designed to test a modified version of the mutual-inductance particle velocity gage to assess its potential for use in the very-high-stress range.

3654-6-1 An experimental nonconducting projectile made from nylon and syntactic foam with a Lucalox head was accelerated to 1200 m/s in the SRI 102 mm-bore gas gun.

Results: The projectile broke up in flight and no useful data were obtained.

3654-6-2 A standard aluminum gas gun projectile, modified by the addition of a 51 mm-long Lucalox-faced plexiglas head extension, was accelerated to 773 m/s in the SRI 64 mm-bore gas gun.

Results: The particle velocity gage gave an excellent record, with no evidence of perturbation by the aluminum portion of the projectile.

DISTRIBUTION LIST

DEPARTMENT OF DEFENSE

Director
Defense Advanced Research Projects Agency
ATTN: NMRO
ATTN: PMO
ATTN: STO
ATTN: Tech. Lib.

Defense Documentation Center
12 cy ATTN: TC

Director
Defense Nuclear Agency
ATTN: STSI, Archives
ATTN: DDST
2 cy ATTN: SPSS
3 cy ATTN: STTL, Tech. Lib.

Commander
Field Command
Defense Nuclear Agency
ATTN: FCT
ATTN: FCPR
ATTN: FCTMOF

Chief
Livermore Division, Field Command, DNA
Lawrence Livermore Division
ATTN: FCPRL

DEPARTMENT OF THE ARMY

Dep. Chief of Staff for Rsch., Dev. & Acq.
ATTN: Tech. Lib.

Commander
Harry Diamond Laboratories
ATTN: DRXDO-NP
ATTN: DRXDO-TI, Tech. Lib.

Director
U.S. Army Ballistic Research Labs.
ATTN: DRXBR-X, Julius J. Meszaros
ATTN: AMXBR-TL-IR, J. H. Keefer
ATTN: Tech. Lib., Edward Baicy

Director
U.S. Army Engr. Waterways Exper. Sta.
ATTN: J. K. Ingram
ATTN: F. Hanes
ATTN: Leo Ingram
ATTN: Tech. Lib.
ATTN: William Flathau

Commander
U.S. Army Materiel Dev. & Readiness Cmd.
ATTN: Tech. Lib.

DEPARTMENT OF THE NAVY

Chief of Naval Research
ATTN: Tech. Lib.

Commander
Naval Facilities Engineering Command
ATTN: Tech. Lib.

DEPARTMENT OF THE NAVY (Continued)

Officer-in-Charge
Civil Engineering Laboratory
ATTN: Tech. Lib.
ATTN: R. J. Odello

Commander
Naval Ship Engineering Center
ATTN: Tech. Lib.

Commander
Naval Ship Rsch. & Development Ctr.
ATTN: Code L42-3, Library

Commander
Naval Ship Rsch. & Development Ctr.
Underwater Explosive Research Division
ATTN: Tech. Lib.

Commander
Naval Surface Weapons Center
ATTN: Code WX-21, Tech. Lib.
ATTN: Code WA-501, Navy Nuc. Prgms Off.

DEPARTMENT OF THE AIR FORCE

AF Geophysics Laboratory, AFSC
ATTN: SUOL, AFCRL, Rsch. Lib.

AF Institute of Technology, AU
ATTN: Library, AFIT, Bldg. 640, Area B

AF Weapons Laboratory, AFSC
ATTN: DES, M. A. Plamondon
ATTN: SUL
ATTN: DEX, J. Renick
ATTN: DEX

HQ USAF/IN
ATTN: INATA

ENERGY RESEARCH & DEVELOPMENT ADMINISTRATION

University of California
Lawrence Livermore Laboratory
ATTN: Tech. Info., Dept. L-3

Sandia Laboratories
Livermore Laboratory
ATTN: Doc. Con. for Tech. Lib.

Sandia Laboratories
ATTN: Doc. Con. for Luke J. Vortman
ATTN: Doc. Con. for A. J. Chaban
ATTN: Doc. Con. for Org. 3422-1, Sandia Rpt. Coll

U.S. Energy Research & Development Administration
Albuquerque Operations Office
ATTN: Doc. Con. for Tech. Lib.

U.S. Energy Research & Development Administration
Division of Headquarters Services
ATTN: Doc. Con. for Class. Tech. Lib.

U.S. Energy Research & Development Administration
Nevada Operations Office
ATTN: Doc. Con. for Tech. Lib.

ENERGY RESEARCH & DEVELOPMENT ADMINISTRATION (Continued)

Union Carbide Corporation
Holifield National Laboratory
ATTN: Civ. Def. Res. Proj., Mr. Kearny

DEPARTMENT OF DEFENSE CONTRACTORS

Aerospace Corporation
ATTN: Prem N. Mathur
ATTN: Tech. Info. Services

Agbabian Associates
ATTN: M. Agbabian

Artec Associates, Inc.
ATTN: D. W. Baum

Civil/Nuclear Systems Corp.
ATTN: Robert Crawford

EG&G, Inc.
Albuquerque Division
ATTN: Tech. Lib.

General Electric Company
TEMPO-Center for Advanced Studies
ATTN: DASIAC

IIT Research Institute
ATTN: Tech. Lib.

Kaman Sciences Corporation
ATTN: Donald C. Sachs
ATTN: Library

Merritt Cases, Incorporated
ATTN: Tech. Lib.
ATTN: J. L. Merritt

The Mitre Corporation
ATTN: Library

Nathan M. Newmark
Consulting Engineering Services
ATTN: W. Hall
ATTN: Nathan M. Newmark

DEPARTMENT OF DEFENSE CONTRACTORS (Continued)

Physics International Company
ATTN: Doc. Con. for Coye Vincent
ATTN: Doc. Con. for Charles Godfrey
ATTN: Doc. Con. for Tech. Lib.
ATTN: Doc. Con. for Fred M. Sauer

R & D Associates
ATTN: J. G. Lewis
ATTN: Tech. Lib.
ATTN: Bruce Hartenbaum

Science Applications, Inc.
ATTN: Tech. Lib.

Southwest Research Institute
ATTN: A. B. Wenzel
ATTN: Wilfred E. Baker

Stanford Research Institute
ATTN: Burt R. Gaston
ATTN: George R. Abrahamson
ATTN: P. S. De Carli

Systems, Science & Software, Inc.
ATTN: Tech. Lib.
ATTN: Donald R. Grine

TRW Systems Group
ATTN: Tech. Info. Ctr., S-1930
2 cy ATTN: Peter K. Dai, RI-2170

TRW Systems Group
San Bernardino Operations
ATTN: E. Y. Wong, 527/712

The Eric H. Wang Civil Engineering Rsch. Fac.
ATTN: Neal Baum
ATTN: G. Lane

Weidlinger Assoc. Consulting Engineers
ATTN: Melvin L. Baron

Weidlinger Assoc. Consulting Engineers
ATTN: J. Isenberg